Optimization and Engineering
https://doi.org/10.1007/s11081-023-09844-6

RESEARCH ARTICLE

Optimizing microgrid deployment for community resilience

James Grymes[1] · Alexandra Newman[1] · Zana Cranmer[2] · Destenie Nock[3]

Received: 6 May 2023 / Revised: 27 August 2023 / Accepted: 27 August 2023

Abstract

The ability to (re)establish basic community infrastructure and governmental functions, such as medical and communication systems, after the occurrence of a natural disaster rests on a continuous supply of electricity. Traditional energy-generation systems consisting of power plants, transmission lines, and distribution feeders are becoming more vulnerable, given the increasing magnitude and frequency of climate-related natural disasters. We investigate the role that fuel cells, along with other distributed energy resources, play in post-disaster recovery efforts. We present a mixed-integer, non-linear optimization model that takes load and power-technology data as inputs and determines a cost-minimizing design and dispatch strategy while considering operational constraints. The model fails to achieve gaps of less than 15%, on average, after two hours for realistic instances encompassing five technologies and a year-long time horizon at hourly fidelity. Therefore, we devise a multi-phase methodology to expedite solutions, resulting in run times to obtain the best solution in fewer than two minutes; after two hours, we provide proof of near-optimality, i.e., gaps averaging 5%. Solutions obtained from this methodology yield, on average, an 8% decrease in objective function value and utilize fuel cells three times more often than solutions obtained with a straight-forward implementation employing a commercial solver.

✉ Alexandra Newman
anewman@mines.edu

James Grymes
jgrymes@mines.edu

Zana Cranmer
acranmer@bentley.edu

Destenie Nock
dnock@andrew.cmu.edu

[1] Mechanical Engineering, Colorado School of Mines, 1500 Illinois St., Golden, CO 80401, USA

[2] Natural and Applied Sciences, Bentley University, 175 Forest St., Waltham, MA 02452, USA

[3] Engineering and Public Policy Department, Carnegie Mellon University, 5000 Forbes Ave, Pittsburgh, PA 15213, USA

Journal: **11081** Article No.: **9844** TYPESET DISK LE CP Disp.:**2023/10/21** Pages: **35** Layout: **Small-Ex**

Keywords Microgrid · Solid oxide fuel cell · Resilience · Non-linear optimization

1 Introduction and background

Climate-related events that contribute to power disruptions are becoming more widespread. In 2021, the U.S. encountered 20 separate billion-dollar weather- and climate-related disasters, almost all of which impacted the ability to deliver reliable electricity to communities. The U.S. Department of Energy defines reliability as the ability of the system or its components to withstand instability, uncontrolled events, cascading failures, and/or unanticipated loss of system components. The Federal Energy Regulatory Commission defines resilience as “the capacity to anticipate, adapt to, and rapidly recover from disruptive incidents.”

An independent group of scientists and communicators who research climate change reports a 67% increase in major power outages between the first and second decades of the 2000 s (Climate Central 2020); Fig. 1 reflects the costs associated with increased climate-related disasters. The average annual cost over the five-year period between 2017 and 2021 constituted $148.4 billion, a new record (Smith 2021). The Department of Energy (2018) estimates that power outages cost the U.S. economy $150 billion per year and disruptions to power infrastructure are more attributable to climate-related events than to any others (Fig. 2). To protect large-scale infrastructure, utilities often deploy power safety shutoff measures which, without backup power generation, threaten the safety and well-being of residents. Thus, having a policy that provides reliable, affordable electricity in post-disaster recovery efforts will become more pressing, especially because the number of natural disasters is expected to rise (Schoennagel et al. 2017; Chapin et al. 2008).

The nature and severity of natural disasters may require residents either to *shelter-in-place* or to evacuate. Examples of the latter include hurricanes and large-scale fires during which the deployment of rescue and response teams to the impacted area is a higher priority than maintaining persistent power (Kocatepe et al. 2019). Wildfires are particularly menacing due to their non-predictive nature. Climate-related impacts, such as droughts and heatwaves, have increased global wildfire risk (Davies et al.

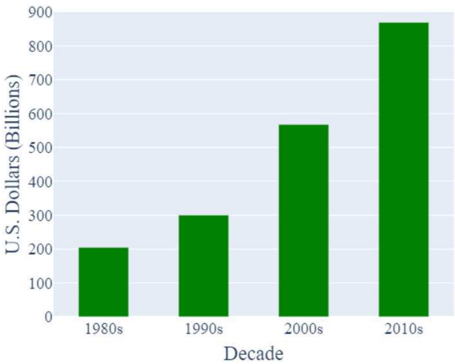

Fig. 1 Climate-related disaster costs by decade (Smith 2021). See Appendix A for a description of cost types included

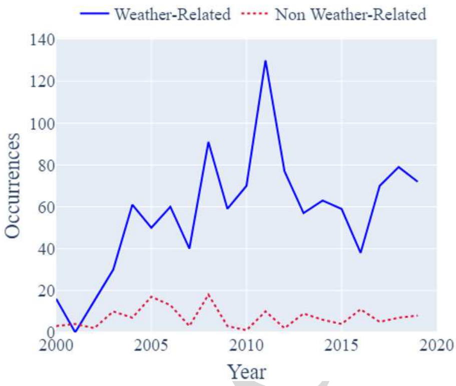

Fig. 2 Number of power outages affecting more than 50,000 customers (U.S. Department of Energy 2023)

2018; Jolly et al. 2015; Zolan et al. 2021). In 2017, over 71,000 wildfires burned 10 million acres and more than 12,000 structures (Jenkins 2018). Within the U.S., 29 million Americans live with the significant potential for extreme wildfires (USAToday 2018). Fire-related events pose risks to both the power generation and the distribution system, which include transmission and distribution lines (Campbell 2012). The area impacted by wildfires often encompasses multiple types of power system architectures in which the effects differ by the level (i.e., electricity delivery and generation) of electrical equipment. At low-voltage (i.e., residential) delivery, a fire may cause system components to fail; conversely, high-voltage transmission components may be more resilient (Donaldson et al. 2020). Some electrical service disruptions are due to preventative measures enacted by the utility service to prevent wildfires. For example, in 2019, Pacific Gas and Electric's planned power shutoffs left an estimated 2.7 million people devoid of electricity, possibly the state's largest planned blackout ever (Newburger 2019).

In addition to economic implications, there are social implications related to vulnerable populations (e.g., the elderly and those with electricity-dependent health risks) such as their inability to evacuate (Greene and Hammerschlag 2000; Molinari et al. 2017; Palaiologou et al. 2019). In 2017, over 65% of victims in the Northern Californian fire were over the age of 65 (Palaiologou et al. 2019). Regardless of whether power outages are caused by fire-related damage to the power system (i.e., generation and transmission) or are due to preventative measures, communities depend on energy for infrastructure such as hospitals.

Due to the dependence of many first-world countries on electricity for communication, healthcare, and water purification, efforts at the federal level are directed toward reducing electrical downtime. Many utilities are investing in distributed generation to improve network reliability and resilience with proper consideration of technology mix, size, and placement. Abiodun et al. (2022) document how distributed generation can enhance power system resilience and improve energy equity. However, conventional microgrids, which often include technologies such as diesel generators, produce unhealthy exhaust, resulting in those with preexisting health conditions suffering consequences from resulting air pollution exposure. Fuel cells address this concern in that they run without emitting fumes, particulates, or carbon monoxide; and, because

Journal: 11081 Article No.: 9844 TYPESET DISK LE CP Disp.:2023/10/21 Pages: 35 Layout: Small-Ex

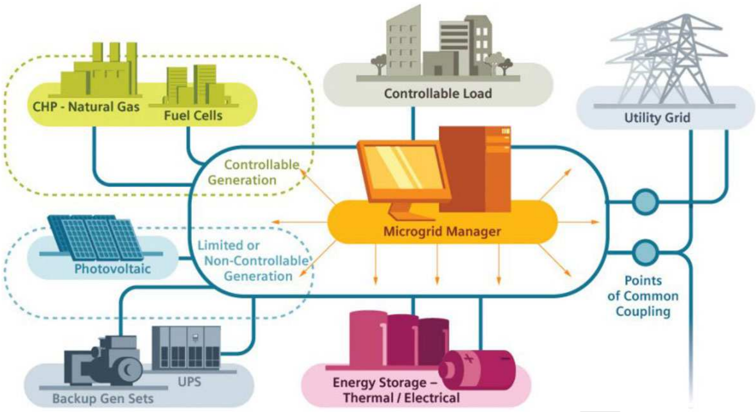

Fig. 3 A representative microgrid and energy system (Center for Climate and Energy Solutions 2020)

of this, fuel cells can be housed within a building, protecting it from some climate-disaster-related risks.

We develop an optimization model that prescribes an appropriate configuration and size of a distributed generation system to provide communities, in an environmentally sound way, with critical services during an electrical service disruption. Figure 3 depicts a traditional microgrid consisting of fossil-fuel powered combined-heat-and-power systems, reciprocating engine generators, and solar power combined with electrical storage (Center for Climate and Energy Solutions 2020). The microgrid market in the U.S., with 10 gigawatts of installed capacity in 2022, is projected to grow by 19% annually through 2027, with disaster mitigation being a primary use case (Nilsson 2023).

While microgrids provide electricity resilience, threats to these types of systems include physical destruction to solar panels (through wind, fire, and hail), damage to electrical storage systems from extreme temperatures, and harmed fuel delivery systems (Mishra et al. 2020). Donaldson et al. (2020) show that the presence of distributed roof-top solar and wind turbines has increased the exposure of electricity generation equipment to wildfires. The corresponding risk continues to grow as more homes (and, subsequently, electrical infrastructure) are built using renewable technologies and at the wildland-urban interface. Deliberate consideration of technologies, their vulnerabilities, and their construction mitigates these threats. For example, Anderson et al. (2023a) show that during a hurricane-induced outage, the inclusion of combined-heat-and-power technologies at a wastewater treatment facility increases the overall resilience of the system through its ability to burn on-site biofuel. The same benefit would not be realized with a traditional microgrid. Beigzadeh et al. (2021) demonstrate that fuel cells can deliver on-demand energy sourced from industrial-waste biogas, syngas, biofuel, and gasified biomass. The ability to operate with on-site fuel yields a microgrid design with solid oxide fuel cells that possess the ability to continuously operate even if the fuel supply is disrupted. We incorporate solid oxide fuel cell technology into microgrid design to reduce these vulnerabilities and to ensure that dependable energy sources exist.

Journal: 11081 Article No.: 9844 TYPESET DISK LE CP Disp.:2023/10/21 Pages: 35 Layout: Small-Ex

2 Literature review

There is an abundance of literature that addresses microgrid design, microgrid dispatch, and power system reliability and resilience. The fundamental gap in our knowledge and ability to deploy these technologies stems from a void of techno-economic microgrid optimization models addressing energy resilience and environmentally friendly, deployable technologies such as fuel cells. HOMER (Hybrid Optimization Model for Electric Renewables), a widely used design and dispatch program, is a simulation model that, for a year-long demand profile, uses fixed dispatch strategies and ranks resulting solutions based on life-cycle cost (Lambert 2000; Rehman and Al-Hadhrami 2010). Some models employ prescriptive (optimization) methods; we highlight a few examples. A mixed-integer program with wind power, batteries, and generators produces results comparable to HOMER's (Aziz et al. 2022); however, their model generates the following solutions sequentially: (1) procurement resulting from running the mixed-integer program for a curtailed time horizon; and, (2) dispatch following from a data mining algorithm to determine an operations strategy for the entire year given procurement from (1).

A two-phase approach fails to coordinate dispatch decisions and procurement strategies. Another techno-economical model, REopt® (Anderson et al. 2017), is a cost-minimizing deterministic mixed-integer linear program that yields an optimal design and dispatch of distributed energy resources, including gas turbines, renewables, and energy storage systems, to meet a set of predefined electrical, thermal, and cooling loads. While this model determines design and dispatch concurrently, it does not include solid oxide fuel cells, nor does it consider the non-linearities associated with thermal storage.

Pruitt et al. (2014) develop a nonconvex, mixed-integer, nonlinear program to prescribe the design and dispatch of a distributed generation system of combined heat and power using solid oxide fuel cells for commercial buildings for a time horizon of one year at hourly fidelity. This model does not incorporate utility-related outages and omits technologies such as gas-turbine combined-heat-and-power systems and backup diesel generators; solutions to instances with time horizons that extend beyond a month are cost-minimizing only when all power is sourced exclusively from the grid. Some authors explore similar frameworks and reduce complexity by shortening the time horizon (Morais et al. 2010) or by using identical daily demands (Bernal-Agustín et al. 2006). Other optimization models that incorporate solid oxide fuel cells as part of their system either: (1) omit the design or detailed dispatch component (Qazi et al. 2018; Sorrentino et al. 2019), and/or (2) use heuristics, rather than exact techniques, to determine a solution (Vigneysh and Kumarappan 2016; Deng et al. 2011). Arefifar et al. (2013) optimize microgrid design under considerations of reliability and supply security. Shokoohi et al. (2018) examine controls in smart grids in line with Lin et al. (2018), who review various strategies in the implementation of power system resilience. To lessen the health impacts and damages associated with, for example, wildfires, Pacific Gas and Electric (California's largest public utility) has proposed to deploy decentralized generation such as solar panels and diesel generators (Pacific Gas and Electric 2021). Similarly, Scioletti et al. (2017) examine such a microgrid including batteries, and Goodall et al. (2019) extend this system to capture battery

Journal: 11081 Article No.: 9844 TYPESET DISK LE CP Disp.:2023/10/21 Pages: 35 Layout: Small-Ex

fade. However, these applications miss an opportunity to utilize emerging, clean technologies, such as solid oxide fuel cells, to support critical entities such as hospitals and community centers.

Our research contributes to the literature by creating cost-minimizing, distributed generation solutions, including solid oxide fuel cells, while considering utility-service disruptions attributable to a natural disaster-induced outage. Specifically, our focus is disasters that result in a significant portion of the population remaining in place and relying on energy for sustainment and recovery. Our optimization framework considers how fuel cells, combined with other distributed generation, can reduce electrical outage time post-wildfire and support community rebuilding. We first describe individual components and then present a mathematical formulation of the entire system. The resulting output is a cost-minimizing system that prescribes the size of the solid oxide fuel cells, as well as conventional, renewable, and co-generational technologies, to provide planners with viable resilience solutions. We embellish a design and dispatch optimization model through enhancements that include: (1) additional generational technologies, (2) new procurement costs, (3) modifications to the electrical storage systems, and (4) technology-specific modeling assumptions. We expand knowledge and capabilities in the disaster-response-and-recovery literature by creating a tool that can analyze and evaluate the value of different technology mixes (i.e., solar and storage, fuel cells, and gas-turbine generators) for a microgrid. Our model accounts for on-site heating loads to demonstrate the co-generational contributions of the technology mix. We capture the temporal and seasonal nature of energy demand, and create a cost-benefit framework for the responsible civic organization. We investigate the specific contribution that solid oxide fuel cells make in delivering energy services due to their co-generational capability and ability to be sourced by a variety of fuel types, including bio-waste (Baldinelli et al. 2021). We provide decision-makers with solutions that would allow electric utilities to respond to disasters (i.e., wildfires and earthquakes) that have a high probability of causing blackouts.

3 Modeling the energy system

Our optimization model, ($\mathcal{P}'$), extended from Pruitt et al. (2014), investigates how microgrids bring reliability and resilience to communities post-disaster (Fig. 4). We incorporate a grid-related outage and additional co-generational technologies. We consider a simulated set of electrical loads, of various quantities, for a distribution feeder. The installed microgrid is co-located at a building site with a thermal load. We incorporate characteristics of the technologies, such as efficiencies and start-up requirements. We utilize basic utility rate structures that include both energy and peak demand charges. The objective minimizes total cost, consisting of the capital, operations and maintenance (O&M), and operational costs of the acquired technologies, as well as the existing costs resulting from demand met by the utility and on-site hot-thermal energy system, typically, a boiler. We include an emissions penalty in the objective function. Design variables associated with fuel cells are general integers to assist with modeling the hourly operation of the system. We relax integrality on all other procurement variables. We assume that all design decisions are made at the beginning of the

Journal: 11081 Article No.: 9844 TYPESET DISK LE CP Disp.:2023/10/21 Pages: 35 Layout: Small-Ex

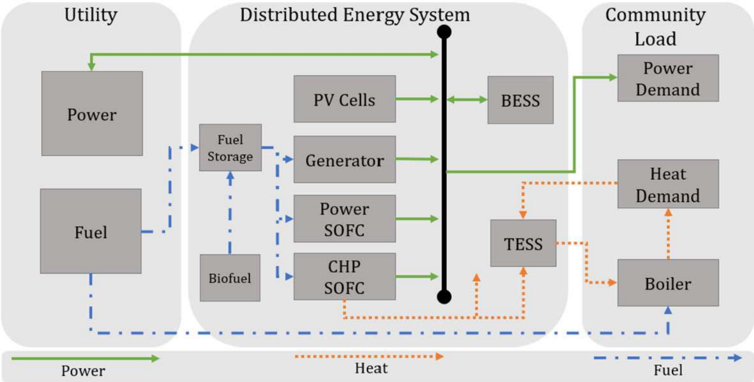

Fig. 4 Distributed energy system modified from Pruitt et al. (2014). *Note*: CHP: combined heat and power, BESS: battery electric storage system, TESS: thermal energy storage system, PV: photovoltaic

time horizon. The model includes both linear and non-linear constraints. We present the full mathematical formulation ($\mathcal{P}'$) in Sect. 3.1.

We utilize capital and lower-case letters to distinguish variables and parameters, respectively. We use script capital letters to distinguish sets, subsets, and indexed sets. Additionally, notation with check and hat decorations describes flows in and out of an entity, respectively. Variables X, Y, and Z represent continuous, integer, and binary quantities, respectively.

3.1 Mathematical formulation

Sets		
$\mathcal{K}$	Technology cost segments	
$\mathcal{J}$	Power producing technologies	
$\mathcal{M}$	Months of year	
$\mathcal{T}$	Time steps	
Subsets and indexed sets		
$\mathcal{J}^{\mathrm{S}} \subseteq \mathcal{J}$	Solid oxide fuel cell technologies	
$\mathcal{J}^{\mathrm{CHP}} \subseteq \mathcal{J}$	Combined heat and power technologies	
$\mathcal{J}^{\mathrm{R}} \subseteq \mathcal{J}$	Renewable technologies	
$\mathcal{J}^{\mathrm{B}} \subseteq \mathcal{J}$	Heat-only producing technologies	
$\mathcal{J}^{\mathrm{E}} \subseteq \mathcal{J}$	Electrical producing technologies	
$\mathcal{T}_m \subseteq \mathcal{T}$	Time steps in month m	
$\mathcal{T}^{\mathrm{g}} \subseteq \mathcal{T}$	Time steps when the utility is available	
Time and demand parameters		
Δ	Demand time steps	[hours]
d_t^{h}	Heating load in time step t	[kW]
d_t^{p}	Electric load in time step t	[kW]

Journal: 11081 Article No.: 9844 TYPESET DISK LE CP Disp.:2023/10/21 Pages: 35 Layout: Small-Ex

Cost and emission parameters

κ_j	Annualized variable capital cost of technology j	[$/unit]
κ^{a}_{jk}	Annualized fixed installation cost of technology j in size segment k	[$]
κ^{b}	Annualized variable capital cost of electric battery	[$/kWh]
κ^{w}	Annualized variable capital cost of water storage	[$/gal]
c^{om}_j	Operation and maintenance cost of technology j	[$/kWh]
c^{p}_t	Utility energy cost (including emissions penalty) in time step t	[$/kWh]
c^{s}_t	Utility energy purchase price in time step t	[$/kWh]
c^{g}_t	Utility gas cost (including emissions penalty) in time step t	[$/kWh]

Power generation and storage parameters

$\bar{b}_{jk}$	Maximum power rating of technology j in cost segment k	[kW]
$\overline{\eta}^{\mathrm{e}}_j$	Maximum electricity efficiency for technology j	[fraction]
$\underline{\eta}^{\mathrm{e}}_j$	Minimum electricity efficiency for technology j	[fraction]
$\overline{\eta}^{\mathrm{b}}$	Maximum electricity efficiency for technology electrical storage	[fraction]
$\hat{k}_j$	Power rating of technology j	[kW/unit]
f^{b}_j	y-intercept for fuel of technology j	[unitless]
f^{m}_j	Fuel burn slope of technology j	[unitless]
f^{p}_{jt}	Production factor of technology j in time step t	[fraction]
μ_j	Maximum turn-down of technology j	[fraction]
ψ_j	Amount of fuel needed to start up technology j	[kWh/unit]
$\underline{s}$	Minimum capacity of electrical storage system	[fraction]
$\overline{s}$	Maximum capacity of electrical storage system	[fraction]
σ_j	Start-up time for each technology j to reach maximum turn-down (μ_j)	[hours]

Heat generation and storage parameters

α	Ambient heat loss for water	[fraction]
ϵ	Arbitrary temperature for which there is no thermal loss	[°C]
η^{h}_j	Thermal efficiency for technology j	[fraction]
γ_j	Exhaust gas output for technology j	[kg/kWh]
h^{e}	Specific heat of exhaust	[kWh/(kg °C)]
h^{w}	Specific heat of water	[kWh/(gal °C)]
$\overline{\nu}$	Maximum water storage capacity	[gal]
$\underline{\nu}$	Minimum water storage capacity	[gal]
$\hat{\tau}_j$	Average exhaust temperature from hot-thermal-producing technology j	[°C]
$\check{\tau}$	Average return water temperature to water storage tank	[°C]
$\overline{\tau}$	Maximum allowed temperature of water in the system	[°C]
$\underline{\tau}$	Minimum allowed temperature of water in the system	[°C]

Journal: **11081** Article No.: **9844** TYPESET DISK LE CP Disp.:**2023/10/21** Pages: **35** Layout: **Small-Ex**

Continuous variables

X^{w}	Volume of water storage tank	[gal]
X^{ba}	Amount of electrical storage procured	[kWh]
$\hat{X}^{\mathrm{u}}_t$	Power purchased from the utility in time step t	[kW]
$\check{X}^{\mathrm{u}}_t$	Power sold to the utility in time step t	[kW]
$\bar{X}^{\mathrm{u}}_m$	Peak power purchased from the utility in month m	[kW]
X^{p}_{jt}	Power produced by each technology j in time step t	[kW]
$\check{X}^{\mathrm{b}}_t$	Power into electrical storage system in time step t	[kW]
$\hat{X}^{\mathrm{b}}_t$	Power out of electrical storage system in time step t	[kW]
X^{bsc}_t	State of charge of electrical storage system in time step t	[kWh]
X^{ef}_{jt}	Electric efficiency of each technology j in time step t	[fraction]
X^{f}_{jt}	Fuel consumed by technology j in time step t	[kW]
$\check{X}^{\mathrm{fl}}_{jt}$	Flow rate of fluid into thermal storage from technology j in time step t	[kg/hour]
$\hat{X}^{\mathrm{fl}}_t$	Flow rate of water out of thermal storage in time step t	[gal/hour]
X^{t}_t	Temperature of water in storage in time step t	[°C]

Integer variables

Y^{a}_j	Number of each technology j procured	[units]
Y^{op}_{jt}	Number of each technology j operating in time step t	[units]
Y^{to}_{jt}	Increased number of each technology j operating from $t-1$ to t	[units]

Binary variables

Z^{ak}_{jk}	1 if generating technology j in segment k is procured, 0 otherwise	[binary]
Z^{w}	1 if additional water storage capacity is procured, 0 otherwise	[binary]
$\check{Z}^{\mathrm{t}}_t$	1 if water storage tank is above $(\check{\tau}+\epsilon)$ in time step t, 0 otherwise	[binary]
$\hat{Z}^{\mathrm{t}}_t$	1 if water storage tank is above $(\hat{\tau}_{\mathrm{boiler}})$ in time step t, 0 otherwise	[binary]

Objective function (See Sect. 3.2.1)

$$
\begin{aligned}
(\mathcal{P}')\quad \text{minimize}\quad & \underbrace{\kappa^b X^{\mathrm{ba}} + \sum_{j\in\mathcal{J},k\in\mathcal{K}} \kappa^{\mathrm{a}}_{jk} Z^{\mathrm{ak}}_{jk} + \sum_{j\in\mathcal{J}} \kappa_j Y^{\mathrm{a}}_j + \kappa^{\mathrm{w}}(X^{\mathrm{w}} - \underline{\nu})}_{\text{Capital Costs}} \\
& + \Delta \underbrace{\sum_{j\in\mathcal{J}^{\mathrm{E}},t\in\mathcal{T}} c^{\mathrm{om}}_j X^{\mathrm{p}}_{jt}}_{\text{O\&M Costs}} + \underbrace{\sum_{j\in\mathcal{J}^{\mathrm{S}},t\in\mathcal{T}} c^{\mathrm{g}}_t(\psi_j Y^{\mathrm{to}}_{jt} + \Delta X^{\mathrm{f}}_{jt})}_{\text{Fuel Costs}} \\
& + \Delta \underbrace{\sum_{t\in\mathcal{T}} c^{\mathrm{p}}_t \hat{X}^{\mathrm{u}}_t + \sum_{m\in\mathcal{M}} c^{\mathrm{d}}_m \bar{X}^{\mathrm{u}}_m}_{\text{Grid Purchase}} - \Delta \underbrace{\sum_{t\in\mathcal{T}} c^{\mathrm{s}}_t \check{X}^{\mathrm{u}}_t}_{\text{Grid Sales}} \\
& + \Delta \underbrace{\sum_{j\in\mathcal{J}^{\mathrm{B}},t\in\mathcal{T}} (\eta^{\mathrm{h}}_j c^{\mathrm{om}}_j + c^{\mathrm{g}}_t) X^{\mathrm{f}}_{jt}}_{\text{Existing Boiler Cost}} \qquad (1)
\end{aligned}
$$

Journal: 11081 Article No.: 9844 TYPESET DISK LE CP Disp.:2023/10/21 Pages: 35 Layout: Small-Ex

Load balancing (See Sect. 3.2.2)

$$(\bar{\eta}^{\mathrm{b}}\hat{X}^{\mathrm{b}}_t - \check{X}^{\mathrm{b}}_t) + \sum_{j\in\mathcal{J}^{\mathrm{E}}} X^{\mathrm{p}}_{jt} + (\hat{X}^{\mathrm{u}}_t - \check{X}^{\mathrm{u}}_t) = d^{\mathrm{p}}_t \quad \forall t \in \mathcal{T}^{\mathrm{g}} \tag{2a}$$

$$(\bar{\eta}^{\mathrm{b}}\hat{X}^{\mathrm{b}}_t - \check{X}^{\mathrm{b}}_t) + \sum_{j\in\mathcal{J}^{\mathrm{E}}} X^{\mathrm{p}}_{jt} = d^{\mathrm{p}}_t \quad \forall t \in \mathcal{T} \setminus \mathcal{T}^{\mathrm{g}} \tag{2b}$$

$$h^{\mathrm{w}}(\hat{\tau}_j - \check{\tau})\hat{X}^{\mathrm{fl}}_t\left[\left(1-\left[1-\frac{\hat{\tau}_j - \underline{\tau}}{X^{\mathrm{t}}_t - \underline{\tau}}\right]\hat{Z}^{\mathrm{t}}_t\right)^{-1}\right] = d^{\mathrm{h}}_t \quad \forall j \in \mathcal{J}^{\mathrm{B}}, t \in \mathcal{T} \tag{2c}$$

Utility operations (See Sect. 3.2.3)

$$\bar{X}^{\mathrm{u}}_m \geq \hat{X}^{\mathrm{u}}_t \quad \forall m \in \mathcal{M}, t \in \mathcal{T}_m \tag{3a}$$

$$\sum_{t\in\mathcal{T}_m} \check{X}^{\mathrm{u}}_t \leq \sum_{t\in\mathcal{T}_m} \hat{X}^{\mathrm{u}}_t \quad \forall m \in \mathcal{M} \tag{3b}$$

Power capacity (See Sect. 3.2.4)

$$X^{\mathrm{p}}_{jt} \leq f^{\mathrm{p}}_{jt}\hat{k}_j Y^{\mathrm{a}}_j \quad \forall j \in \mathcal{J}^{\mathrm{R}}, t \in \mathcal{T} \tag{4a}$$

$$\mu_j \hat{k}_j Y^{\mathrm{op}}_{jt} \leq X^{\mathrm{p}}_{jt} \leq \hat{k}_j Y^{\mathrm{op}}_j \quad \forall j \in \mathcal{J}^{\mathrm{E}} \setminus \mathcal{J}^{\mathrm{R}}, t \in \mathcal{T} \tag{4b}$$

$$Y^{\mathrm{op}}_{jt} \leq Y^{\mathrm{a}}_j \quad \forall j \in \mathcal{J}^{\mathrm{S}}, t \in \mathcal{T} \tag{4c}$$

$$\hat{k}_j Y^{\mathrm{a}}_j \leq \bar{b}_{jk} Z^{\mathrm{ak}}_{jk} \quad \forall j \in \mathcal{J}, k \in \mathcal{K} \tag{4d}$$

$$\sum_{k\in\mathcal{K}} Z^{\mathrm{ak}}_{jk} \leq 1 \quad \forall j \in \mathcal{J} \tag{4e}$$

Electricity efficiency (See Sect. 3.2.5)

$$X^{\mathrm{ef}}_{jt} = \left(\frac{\bar{\eta}^{\mathrm{e}}_j - \mu_j \underline{\eta}^{\mathrm{e}}_j}{1-\mu_j}\right) - \left(\frac{\bar{\eta}^{\mathrm{e}}_j - \underline{\eta}^{\mathrm{e}}_j}{\hat{k}_j(1-\mu_j)}\right)\left(\frac{X^{\mathrm{p}}_{jt}}{Y^{\mathrm{op}}_{jt}}\right) \quad \forall j \in \mathcal{J}^{\mathrm{S}}, t \in \mathcal{T} \tag{5}$$

Fuel consumption (See Sect. 3.2.6)

$$X^{\mathrm{f}}_{jt} = \frac{X^{\mathrm{p}}_{jt}}{X^{\mathrm{ef}}_{jt}} \quad \forall j \in \mathcal{J}^{\mathrm{S}}, t \in \mathcal{T} \tag{6a}$$

$$X^{\mathrm{f}}_{jt} = f^{\mathrm{b}}_j \hat{k}_j Y^{\mathrm{op}}_j + f^{\mathrm{m}}_j X^{\mathrm{p}}_{jt} \quad \forall j = \mathcal{J}^{\mathrm{E}} \setminus (\mathcal{J}^{\mathrm{S}} \cup \mathcal{J}^{\mathrm{R}}), t \in \mathcal{T} \tag{6b}$$

$$X^{\mathrm{f}}_{jt} = \frac{h^{\mathrm{w}}\hat{X}^{\mathrm{fl}}_t(\hat{\tau}_j - X^{\mathrm{t}}_t)(1-\hat{Z}^{\mathrm{t}}_t)}{\eta^{\mathrm{h}}_j} \quad \forall t \in \mathcal{T}, j \in \mathcal{J}^{\mathrm{B}} \tag{6c}$$

Start-up (See Sect. 3.2.7)

$$Y^{\mathrm{op}}_{j,t+\sigma_j} - Y^{\mathrm{op}}_{jt} \leq Y^{\mathrm{to}}_{j,t+\sigma_j} \quad \forall j \in \mathcal{J}^{\mathrm{S}}, t \in \mathcal{T} : t < |\mathcal{T}| - \sigma_j \tag{7}$$

Journal: 11081 Article No.: 9844 TYPESET DISK LE CP Disp.:2023/10/21 Pages: 35 Layout: Small-Ex

Power storage (See Sect. 3.2.8)

$$X^{\text{bsc}}_{t+1} - X^{\text{bsc}}_{t} = \Delta(\bar{\eta}^{\text{b}}\check{X}^{\text{b}}_{t} - \hat{X}^{\text{b}}_{t}) \quad \forall t \in \mathcal{T} : t < |\mathcal{T}| \tag{8a}$$

$$\underline{s}X^{\text{ba}} \leq X^{\text{bsc}}_{t} \leq \bar{s}X^{\text{ba}} \quad \forall t \in \mathcal{T} \tag{8b}$$

$$X^{\text{bsc}}_{1} = X^{\text{bsc}}_{|\mathcal{T}|} \tag{8c}$$

Heat capacity (See Sect. 3.2.9)

$$\check{X}^{\text{fl}}_{jt} \leq \gamma_j X^{\text{f}}_{jt} \quad j \in \mathcal{J}^{\text{CHP}}, t \in \mathcal{T} \tag{9}$$

Heat storage (See Sect. 3.2.10)

$$X^{\text{t}}_{t+1} - (1 - \alpha\check{Z}^{\text{t}}_{t})X^{\text{t}}_{t} = \frac{\sum_{j\in\mathcal{J}^{\text{CHP}}}(\Delta\eta^{\text{h}}_{j}h^{\text{e}}\check{X}^{\text{fl}}_{jt}(\hat{\tau}_j - X^{\text{t}}_{t})) - \Delta h^{\text{w}}\hat{X}^{\text{fl}}_{t}(X^{\text{t}}_{t} - \check{\tau})}{h^{\text{w}}X^{\text{w}}} \quad \forall t \in \mathcal{T} : t < |\mathcal{T}| \tag{10a}$$

$$X^{\text{t}}_{t} - \check{\tau} \leq (\bar{\tau} - \check{\tau})Z^{\text{w}} \quad \forall t \in \mathcal{T} \tag{10b}$$

$$\epsilon\check{Z}^{\text{t}}_{t} \leq X^{\text{t}}_{t} - \check{\tau} \leq \epsilon + (\bar{\tau} - \check{\tau} - \epsilon)\check{Z}^{\text{t}}_{t} \quad \forall t \in \mathcal{T} \tag{10c}$$

$$(\check{\tau} - \hat{\tau}_j)(1 - \hat{Z}^{\text{t}}_{t}) \leq X^{\text{t}}_{t} - \hat{\tau}_j \leq (\bar{\tau} - \hat{\tau}_j)\hat{Z}^{\text{t}}_{t} \quad \forall t \in \mathcal{T}, j \in \mathcal{J}^{\text{B}} \tag{10d}$$

$$\underline{\nu} \leq X^{\text{w}} \leq \bar{\nu} \tag{10e}$$

$$Z^{\text{w}} \leq \sum_{j\in\mathcal{J}^{\text{CHP}}} Y^{\text{a}}_{j} \leq \left\lceil \frac{\max_{t\in\mathcal{T}}\{d^{\text{P}}_{t}\}}{\min_{j\in\mathcal{J}^{\text{CHP}}}\{\hat{k}_j\}} \right\rceil Z^{\text{w}} \tag{10f}$$

Non-negativity and integrality

$$X^{\text{w}}, X^{\text{ba}} \geq 0 \tag{11a}$$

$$X^{\text{f}}_{jt}, X^{\text{p}}_{jt}, X^{\text{ef}}_{jt}, \check{X}^{\text{fl}}_{jt} \geq 0 \quad \forall j \in \mathcal{J}, t \in \mathcal{T} \tag{11b}$$

$$\bar{X}^{\text{u}}_{m} \geq 0 \quad \forall m \in \mathcal{M} \tag{11c}$$

$$\hat{X}^{\text{u}}_{t}, \check{X}^{\text{u}}_{t}, \check{X}^{\text{b}}_{t}, \hat{X}^{\text{b}}_{t}, X^{\text{bsc}}_{t}, \hat{X}^{\text{fl}}_{t}, X^{\text{t}}_{t} \geq 0 \quad \forall t \in \mathcal{T} \tag{11d}$$

$$Y^{\text{a}}_{j} \geq 0, \text{integer} \quad \forall j \in \mathcal{J} \tag{11e}$$

$$Y^{\text{op}}_{jt}, Y^{\text{to}}_{jt} \geq 0, \text{integer} \quad \forall j \in \mathcal{J}, t \in \mathcal{T} \tag{11f}$$

$$Z^{\text{w}} \text{ binary} \tag{11g}$$

$$\check{Z}^{\text{t}}_{t}, \hat{Z}^{\text{t}}_{t} \text{ binary} \quad t \in \mathcal{T} \tag{11h}$$

$$Z^{\text{ak}}_{jk} \text{ binary} \quad j \in \mathcal{J}, k \in \mathcal{K} \tag{11i}$$

3.2 Discussion of formulation

We describe, in detail, the objective function and constraint set.

Journal: 11081 Article No.: 9844 TYPESET DISK LE CP Disp.:2023/10/21 Pages: 35 Layout: Small-Ex

3.2.1 Objective function

The objective function minimizes costs associated with fixed and variable procurement, operation and maintenance, power generation, and the net utility charge. Procurement includes both size-dependent capital cost (variable) and installation (fixed), which may incorporate the construction of tailored equipment housing units and the emplacement of piping and cables. The fixed cost segments are increasing and therefore convex, precluding binary logic to ensure placement in the appropriate cost segment. Binary variable Z_{jk}^{ak} enforces the piecewise-linear installation cost. The way in which load is met is influenced by the fuel cost and grid purchase terms in the objective function and controlled through various constraints in set (6).

We use a standard annualized cost computation, which includes the use of a capital recovery factor (Lambert 2000):

$$\kappa_j = \frac{i(1+i)^{N_j}}{(1+i)^{N_j}-1}\bar{\kappa}_j \quad \forall j \in \mathcal{J} \tag{12}$$

where i is the annualized real discount rate, N_j is the expected lifetime, in years, of technology j and $\bar{\kappa}_j$ is the net present capital cost of technology j. Although expression (12) only includes the technologies in set $\mathcal{J}$, this formula is extended to the electrical storage system as well.

3.2.2 Load balancing

Constraint (3.1) balances electrical load with the sum of: the amount of net power deployed from the storage system, the power dispatched from all electrical power systems, and the net power purchased from the utility. We relax, from equality, this constraint by ensuring that the net power produced by the microgrid and purchased from the utility meets or exceeds the electrical load. We introduce a gas turbine generator with and without combined-heat-and-power capabilities to the set $\mathcal{T}^{\mathrm{e}}$, in addition to fuel cells and photovoltaic panels. Constraint (2b) restricts the grid interaction during utility service disruptions, requiring all loads to be met with the microgrid. We enforce constraint (2c) through a set of bi- and tri-linear terms in which the on-site heating load is met through a mixture of hot and cold water. If the water temperature in the tank is above $\hat{\tau}_{\mathrm{Boil}}$, then thermal demand is met through the product of variable water flow out of the tank and the temperature gradient above the delivery temperature. Otherwise, the flow out becomes fixed and is determined by equation (13). As the temperature of the water in the storage tank increases, the flow of water out decreases; and, therefore, the fuel needed to power the boiler decreases (Pruitt et al. 2014).

$$\hat{X}_t^{\mathrm{fl}} = \frac{d_t^{\mathrm{h}}}{h^{\mathrm{w}}(\hat{\tau}_{\mathrm{Boil}} - \check{\tau})} \quad \forall t \in \mathcal{T} \tag{13}$$

Journal: 11081 Article No.: 9844 TYPESET DISK LE CP Disp.:2023/10/21 Pages: 35 Layout: Small-Ex

3.2.3 Utility operations

Constraint (3a) is the linearization of equation (14), which captures the peak power purchased in month m. Constraint (3b) restricts energy arbitrage and enforces net metering, typical for grid-connected systems.

$$\bar{X}^{\mathrm{u}}_m = \max_{\{t \in \mathcal{T}_m\}} \hat{X}^{\mathrm{u}}_t \quad \forall m \in \mathcal{M} \tag{14}$$

3.2.4 Power capacity

Constraint (4a) restricts the power output of renewable technology j to be less than or equal to the product of the capacity of the procured system and the production factor in hour t. Constraint (4b) ensures that the power output of non-renewable, electric-producing technology j is between the minimum required turn-down and the maximum amount of available power in hour t. The former level forces the fuel cell to produce sufficient power at its minimum required temperature. Constraint (4c) restricts the number of operational fuel cells to be no more than the number acquired. Constraint (4d) dictates that the chosen power rating is assigned to the correct installation cost segment. Constraint (4e) limits the selection to at most one segment.

3.2.5 Electrical efficiency

We model electrical efficiency as a decreasing function of the average output of the operational fuel cells through constraint (5). In this case, as the power output increases, the electrical efficiency of the system decreases. We assume that all fuel cells of type j operate identically. The tradeoff, however, is the inclusion of additional bi-linear terms that include the product of a continuous variable and a general integer variable. The variable efficiency is bounded between $\underline{\eta}_j$ and $\bar{\eta}_j$ for fuel cell technology j (Pruitt et al. 2014).

3.2.6 Fuel consumption

Constraint (6a) ensures that the amount of fuel consumed by fuel cell type j in time period t is equal to the quotient of the total power produced and the average variable efficiency; this constraint creates $|\mathcal{J}^{\mathrm{S}}| \cdot |\mathcal{T}|$ additional bi-linear terms. We implement constraint (6b) to compute the fuel needed to produce X^{p}_{jt} kW of power for both the standard electrical and combined-heat-and-power generators. We use the linear formulation consisting of the sum of the marginal contribution of fuel per kW ($f^{\mathrm{m}}_j X^{\mathrm{p}}_{jt}$) and the product of the y-intercept (f^{b}_j) and the capacity of fuel cells operating in a given hour ($\hat{k}_j Y^{\mathrm{op}}_{jt}$). We implement constraint (6c) to calculate the fuel used to power the boiler as the quotient of the amount of thermal energy dispatched and the boiler efficiency. If the water temperature is above the delivery temperature, then no fuel is consumed (Pruitt et al. 2014).

Journal: 11081 Article No.: 9844 TYPESET DISK LE CP Disp.:2023/10/21 Pages: 35 Layout: Small-Ex

3.2.7 Start-up

The coarseness of our chosen time fidelity precludes the necessity of power-ramping constraints; that is, fuel cell operation can fluctuate between the maximum power rating and minimum turn-down within a single time step. However, when activated, solid oxide fuel cells must reach a designated temperature prior to producing power. The parameter σ_j dictates the number of time steps to reach operational temperature from ambient. Therefore, we include constraint (7) to ensure that if the number of fuel cells in operation in time period $t + \sigma_j$ is greater than the number of fuel cells operational in time period t, then Y^{to}_{jt} assumes the value of the difference; otherwise, its value is 0. This models the number of fuel cells required to turn on in time period t and ensures that we capture the amount of time and fuel necessary to bring the fuel cell from ambient to operational temperature prior to dispatching power.

3.2.8 Power storage

Constraint (8a) requires that the difference in states of charge between time steps t and $t + 1$ equal the net energy dispatched from the storage system in time period t. We incorporate a constant electrical efficiency loss for charging the battery. Constraint (8b) dictates that the battery's state of charge is restricted to between the minimum and maximum allowable limit of the procurement variable. Constraint (8c) requires equality of the electrical storage system's beginning and ending state of charge.

3.2.9 Heat capacity

In our system, fuel cells with combined-heat-and-power capabilities provide the added benefit of utilizing the thermal exhaust produced by the fuel cell to heat water in the storage tank. Constraint (9) dictates that the amount of exhaust flow is a function of the fuel consumed by the co-generational fuel cell. We utilize an inequality to allow for curtailment of the thermal energy in time periods in which the inclusion of the exhaust would force the water temperature to exceed its allowable limit. The added co-generational benefit does not apply to diesel-powered generation.

3.2.10 Heat storage

Constraint (10a) governs the temperature differential between time periods. We (i) account for a constant heat loss due to thermal conduction; (ii) add the thermal energy provided by the exhaust heat from the various combined-heat-and-power systems; and, (iii) subtract the thermal energy dispatched to meet the heating load. Constraint (10b) limits the temperature to $\bar{\tau}$ if a storage tank is required and to $\check{\tau}$ otherwise. Constraint (10c) dictates that if the water temperature is arbitrarily close (ϵ) to the return water temperature ($\check{\tau}$), we do not apply the heat loss due to thermal conduction (described in constraint (10a)). Constraint (10d) governs the binary variable $\hat{Z}^{\text{t}}_t$ used to determine if the water temperature is above or below the delivery temperature ($\hat{\tau}_{\text{Boil}}$). Constraint (10f) serves two purposes: (1) it requires the procurement of additional

Journal: **11081** Article No.: **9844** ☐ TYPESET ☐ DISK ☐ LE ☐ CP Disp.:**2023/10/21** Pages: **35** Layout: **Small-Ex**

water storage system capacity if a combined-heat-and-power system is procured; and, (2) it limits the number of acquired combined-heat-and-power systems to the maximum power demand. Constraint (10e) bounds the capacity of the water storage system (Pruitt et al. 2014).

4 Solution methodology

The formulation ($\mathcal{P}'$) is a mixed-integer nonlinear program that includes continuous, binary, and integer variables, as well as constraints with non-linear terms. We measure performance of our problem instances via solution time and optimality gap, the latter of which provides the relative difference between the best integer solution found to the original, nonlinear model and the lower bound derived from convex relaxations of the original, nonconvex problem. State-of-the-art global optimizers yield gaps of greater than 10% after more than two hours of solution time. Therefore, we present, in this section, our methods to expedite solutions to realistic instances of ($\mathcal{P}'$).

Standard approaches include: (1) scaling to reduce the magnitude between the largest and smallest values for each data set; (2) conversion of tri-linear to bi-linear terms and the introduction of auxiliary variables and constraints to create exact linearizations of the product of binary and continuous variables; and, (3) a bound tightening procedure (Pruitt et al. 2014). Through scaling, we reduce the number of orders of magnitude in the data by four. We use standard techniques (Balas 1965) to create exact linearizations of eligible non-linear terms, i.e., nonlinear terms involving the product of at least one discrete variable in which said linearization yields favorable results (see Table 1). By executing the bound-tightening algorithm, we reduce the difference between the upper and lower bounds by more than 50% for select variables.

The full formulation of ($\mathcal{P}'$), after the linearizations reflected in Table 1, has a size reflected in Table 2 and includes $5|\mathcal{T}| + 2|\mathcal{J}^{\mathrm{S}}| \cdot |\mathcal{T}|$ bi-linear terms. We refer to the

Table 1 Type and quantity of non-linear terms in the constraint set and how they are modified after performing standard linearization techniques (Balas 1965)

Type	Term	Quantity	Constraint	Transformation
Bi-linear	$\hat{Z}^{\mathrm{t}}_t X^{\mathrm{t}}_t$	$\lvert\mathcal{T}\rvert$	(2c)	Linear
	$\hat{Z}^{\mathrm{t}}_t \hat{X}^{\mathrm{fl}}_t$	$\lvert\mathcal{T}\rvert$	(6c)	
	$Y^{\mathrm{op}}_{jt} X^{\mathrm{ef}}_{jt}$	$\lvert\mathcal{J}^{\mathrm{S}}\rvert \cdot \lvert\mathcal{T}\rvert$	(5)†	No change
	$X^{\mathrm{ef}}_{jt} X^{\mathrm{f}}_{jt}$	$\lvert\mathcal{J}^{\mathrm{S}}\rvert \cdot \lvert\mathcal{T}\rvert$	(6a)	
	$\hat{X}^{\mathrm{fl}}_t X^{\mathrm{t}}_t$	$\lvert\mathcal{T}\rvert$	(2c), (6c), (10a)	
	$X^{\mathrm{w}} X^{\mathrm{t}}_t$	$\lvert\mathcal{T}\rvert$	(2c)	
	$\check{X}^{\mathrm{fl}}_t X^{\mathrm{t}}_t$	$\lvert\mathcal{T}\rvert$	(2c)	
Tri-linear	$\hat{Z}^{\mathrm{t}}_t \hat{X}^{\mathrm{fl}}_t X^{\mathrm{t}}_t$	$\lvert\mathcal{T}\rvert$	(6c)	Bi-linear
	$\check{Z}^{\mathrm{t}}_t X^{\mathrm{w}} X^{\mathrm{t}}_t$	$\lvert\mathcal{T}\rvert$	(2c)	

†: The case of the product of a continuous and an *integer* (vice binary) variable requires additional model elements for its linearization, and testing yields unfavorable results

Journal: 11081 Article No.: 9844 TYPESET DISK LE CP Disp.:2023/10/21 Pages: 35 Layout: Small-Ex

Table 2 Size of $(\mathcal{P}')$ in terms of set cardinality

Model component	Characteristic	Number
Variables	Continuous	$\lvert\mathcal{T}\rvert \cdot (8 + 3\lvert\mathcal{J}\rvert) + \lvert\mathcal{M}\rvert + 2$
	Integer	$\lvert\mathcal{T}\rvert \cdot (\lvert\mathcal{J}\rvert + 1)$
	Binary	$2\lvert\mathcal{T}\rvert + \lvert\mathcal{J}\rvert \cdot \lvert\mathcal{K}\rvert + 1$
Constraints	Linear	$6\lvert\mathcal{T}\rvert \cdot (1 + \lvert\mathcal{J}\rvert) + \lvert\mathcal{J}\rvert \cdot (1 + \lvert\mathcal{K}\rvert) + \lvert\mathcal{M}\rvert$
	Non-linear	$\lvert\mathcal{T}\rvert \cdot (\lvert\mathcal{J}\rvert + 1)$

Table 3 Constraint numbers with associated quantities required to transform $(\mathcal{P}')$ into $(\mathcal{P}^\ell)$

Model	Energy type	Constraints	Quantity
$(\mathcal{P}')$	Electric	(5), (6a)	$2\lvert\mathcal{J}\rvert \cdot \lvert\mathcal{T}\rvert$
	Thermal	(2c), (6c), (9), (10a)–(10e)	$\lvert\mathcal{T}\rvert(6 + \lvert\mathcal{J}\rvert)$
$(\mathcal{P}^\ell)$	Electric	(15a)–(15g)	$\lvert\mathcal{J}\rvert \cdot \lvert\mathcal{T}\rvert(5\lvert\mathcal{S}\rvert + 1)$
	Thermal	(16a)–(16c)	$3\lvert\mathcal{T}\rvert$

The constraints in each of the rows corresponding to a particular model are mutually exclusive

method of solving $(\mathcal{P}')$ using techniques (1)–(3), outlined in the prior paragraph, as method $(\mathbf{M}^b)$, the **baseline** method. While the implementation of $(\mathbf{M}^b)$ yields optimality gap improvements of approximately 2%, on average, after a two-hour solve time, we are still unable to generate solutions with less than a 10% gap.

Ultimately, complications arise in two sets of constraints: (1) those ensuring that the thermal energy produced through the co-generational technologies and the boiler is sufficient to heat the water in the storage system and meet the hot thermal load (see Table 3: row $(\mathcal{P}')$-Thermal); and, (2) those governing the fuel consumption and the efficiency associated with the solid oxide fuel cells (see Table 3: row $(\mathcal{P}^\ell)$-Electric). Therefore, we present an enhanced, three-phase solution methodology $(\mathbf{M}^e)$, depicted in Fig. 5.

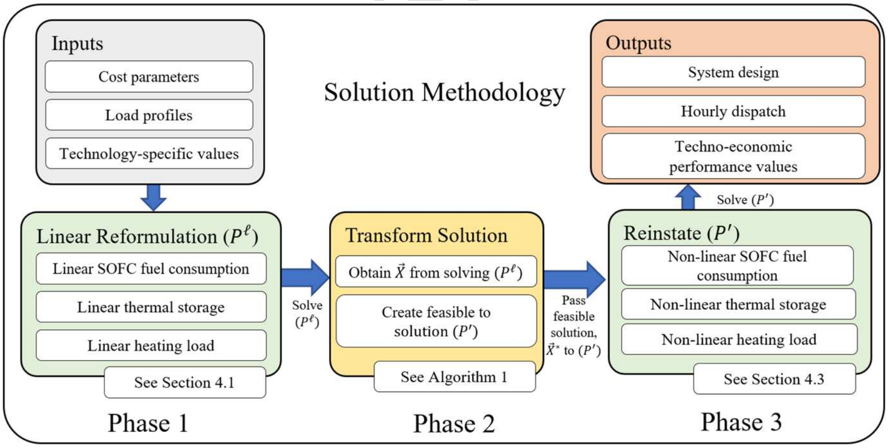

Fig. 5 Three-phase methodology to generate feasible solutions to $(\mathcal{P}')$ with improved solutions and optimality gaps. *Note*: SOFC—solid oxide fuel cell

Journal: 11081 Article No.: 9844 TYPESET DISK LE CP Disp.:2023/10/21 Pages: 35 Layout: Small-Ex

4.1 Linear reformulation (Phase 1)

Phase 1 modifies ($\mathcal{P}'$) by creating linear approximations for constraints in the "no change" and "bi-linear" rows found in Table 1. We refer to this reformulation as ($\mathcal{P}^{\ell}$). Figure 6 depicts a fuel consumption curve, representing a 10kW fuel cell system used in the model ($\mathcal{P}'$), and a linear approximation of that curve. The solid, red curve results from the combination of constraints (5) and (6a), while the dashed, blue line is a piece-wise linear approximation. Without loss of generality, Fig. 6 shows two segments, but the approximation could be made with an arbitrary number of s segments. However, more segments, though potentially providing a more accurate approximation, create additional integer variables and can slow model solve time.

The linear approximation creates a conservative characterization of the system in that the resulting solution is an over-estimation of fuel consumption, resulting in a higher cost of fuel per unit energy produced for the solid oxide fuel cell than when employing the non-linear fuel curve used in ($\mathcal{P}'$). The increased amount of fuel consumed for a commensurate amount of power results in a larger contribution of thermal energy to the heating load. Therefore, the approximation overestimates the total cost, and employing it results in a restriction of our original model ($\mathcal{P}'$).

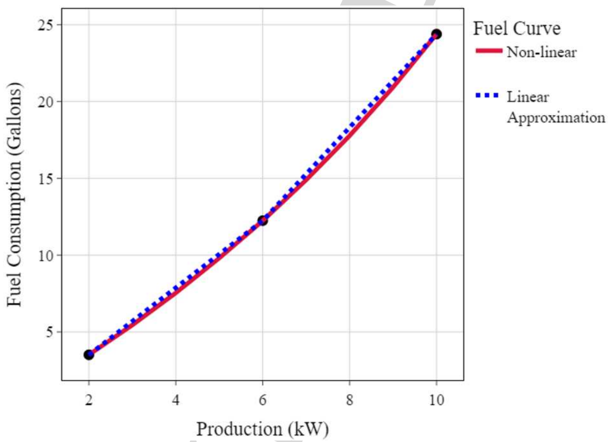

Fig. 6 Comparison of piece-wise linear and non-linear fuel consumption of a representative solid oxide fuel cell with two segments

Journal: **11081** Article No.: **9844** TYPESET DISK LE CP Disp.:**2023/10/21** Pages: **35** Layout: **Small-Ex**

Notation required in model ($\mathcal{P}^{\ell}$):

Notation	Description	Units
$\mathcal{S}$	Linear approximation segments	
b^{f}_{js}	y-intercept for linearization of fuel curve for technology j in segment s	[gal]
m^{f}_{js}	Marginal fuel consumption of technology j for segment s	[gal/kW]
ℓ_{js}	Lower bound of power output of technology j in segment s	[kW]
u_{js}	Lower bound of power output of technology j in segment s	[kW]
Z^{op}_{jst}	1 if technology j is operating in segment s, in time period t and 0 otherwise	[binary]
X^{ps}_{jst}	Amount of power dispatched from technology j in segment s in time period t	[kW]

Fuel cell constraints present in ($\mathcal{P}^{\ell}$):

$$X^{\text{f}}_{jt} \geq m^{\text{f}}_{js} X^{\text{ps}}_{jst} + b^{\text{f}}_{js} Y^{\text{op}}_{jt} - M(1 - Z^{\text{op}}_{jst}) \quad \forall j \in \mathcal{J}^{\text{S}}, s \in \mathcal{S}, t \in \mathcal{T} \tag{15a}$$

$$X^{\text{ps}}_{jst} \geq l_{js} Y^{\text{op}}_{jt} - M(1 - Z^{\text{op}}_{jst}) \quad \forall j \in \mathcal{J}^{\text{S}}, s \in \mathcal{S}, t \in \mathcal{T} \tag{15b}$$

$$X^{\text{ps}}_{jst} \leq u_{js} Y^{\text{op}}_{jt} + M(1 - Z^{\text{op}}_{jst}) \quad \forall j \in \mathcal{J}^{\text{S}}, s \in \mathcal{S}, t \in \mathcal{T} \tag{15c}$$

$$X^{\text{ps}}_{jst} \leq M Z^{\text{op}}_{jst} \quad \forall j \in \mathcal{J}^{\text{S}}, s \in \mathcal{S}, t \in \mathcal{T} \tag{15d}$$

$$X^{\text{p}}_{jt} \leq \sum_{s \in \mathcal{S}} X^{\text{ps}}_{jst} \quad \forall j \in \mathcal{J}^{\text{S}}, t \in \mathcal{T} \tag{15e}$$

$$\sum_{s \in \mathcal{S}} Z^{\text{op}}_{jst} \leq 1 \quad \forall j \in \mathcal{J}^{\text{S}}, t \in \mathcal{T} \tag{15f}$$

$$Z^{\text{op}}_{jst} \leq Y^{\text{op}}_{jt} \quad \forall j \in \mathcal{J}^{\text{S}}, s \in \mathcal{S}, t \in \mathcal{T} \tag{15g}$$

Instead of non-linear fuel consumption as a function of the variable efficiency and power output, ($\mathcal{P}^{\ell}$) represents fuel consumption as a linear function of power output and a fixed fuel intercept. Constraint (15a) governs the fuel consumed by the solid oxide fuel cell and is a linear combination of the power produced and an appropriately selected intercept if the fuel cell is operating in segment s, and 0 otherwise. Constraints (15b)–(15d) require that the power produced by technology j in time period t is restricted between the appropriate lower and upper bounds of segment s. We use constraint (15e) to consolidate power from all segments. Constraint (15f) limits the power output to at most one segment, and constraint (15g) restricts the binary variable to 0 if there are no operational fuel cells. We replace constraints (5) and (6a) with constraints (15a)–(15g).

The other sources of non-linearities reside in the thermal load balance constraint (2c) and in the water tank temperature constraint (10a). We devise a way to linearly approximate these constraints such that they represent the thermal load as a convex combination of energy from the boiler and exhaust heat produced by the solid oxide fuel cell (16a). The associated notation and model modifications follow (see constraints (16a)–(16c)).

Journal: 11081 Article No.: 9844 TYPESET DISK LE CP Disp.:2023/10/21 Pages: 35 Layout: Small-Ex

Linear thermal storage notation:

Notation	Description	Units
$\tilde{\nu}$	Incremental increase of water storage tank size	[gal]
X_t^{hts}	Amount of heat sent to storage in time period t	[kWh]
X_t^{hfs}	Amount of heat dispatched from storage in time period t	[kWh]

Linear thermal energy constraints:

$$\sum_{j \in \mathcal{J}^{\text{CHP}}} \gamma_j \eta_j h^{\text{e}} \hat{\tau}_j X_{jt}^{\text{f}} + \sum_{j \in \mathcal{J}^{\text{B}}} \eta_j X_{jt}^{\text{f}} + (X_t^{\text{hfs}} - X_t^{\text{hts}}) \geq d_t^{\text{h}} \quad t \in \mathcal{T} \tag{16a}$$

$$X_t^{\text{tsc}} = (1-\alpha) X_{t-1}^{\text{tsc}} + X_t^{\text{hts}} - X_t^{\text{hfs}} \quad t \in \mathcal{T} \tag{16b}$$

$$X_t^{\text{tsc}} \leq X^{\text{w}} \quad t \in \mathcal{T} \tag{16c}$$

To account for thermal storage, we add variables X_t^{hts} and X_t^{hfs} which model the heat to and from, respectively, the thermal storage system. Constraint (16a) ensures that the heating load is met through a linear combination of thermal energy from the co-generational solid oxide fuel cell, thermal energy generated by the boiler, and thermal energy from the storage system. We account for energy lost in storage through a parameter α. Constraint (16b) balances the thermal energy in storage, and constraint (16c) restricts the energy in storage to the capacity of the system. We replace the constraints found in row $(\mathcal{P}')$ of Table 3 with the constraints in rows labeled $(\mathcal{P}^{\ell})$ to create a mixed-integer linear model.

4.2 Transform solution (Phase 2)

We solve the linear program $(\mathcal{P}^{\ell})$ utilizing state-of-the-art software and obtain a solution to which we refer as $\vec{X}$. Utilizing the heuristic described in Algorithm 1, we obtain from $\vec{X}$ solution $\vec{X}^*$, which is feasible for $(\mathcal{P}')$. We first initialize the variable values according to $\vec{X}$ from $(\mathcal{P}^{\ell})$. We then compute the solid oxide fuel cell efficiency and fuel consumption in each time period using the power produced by the associated technology. We then determine the variable values, such as exhaust flow from the fuel cell and water temperature, corresponding to the thermal load and thermal storage constraints. We establish a starting temperature and related binary variables $\hat{Z}_t^{\text{t}}$ and $\check{Z}_t^{\text{t}}$. With this information and the amount of exhaust $(\hat{X}_{jt}^{\text{fl}})$ from combined heat and power technology j, we compute the remaining variable values. For those associated with thermal storage, we include a condition to handle a solution resulting in a temperature that exceeds $\bar{\tau}$. In those instances, we increase the volume of the hot water storage tank by $\tilde{\nu}$ and re-compute the variable values. Lastly, we update variable bounds using information obtained by the solution $(\vec{X})$. If combined-heat-and-power technologies are not a component in the fixed design, the computation of variables related to thermal load becomes explicit, as shown by **Function 2** found in Algorithm 1.

Journal: 11081 Article No.: 9844 TYPESET DISK LE CP Disp.:2023/10/21 Pages: 35 Layout: Small-Ex

Algorithm 1 Induce feasibility in $(\mathcal{P}')$ from a solution to $(\mathcal{P}^{\ell})$.
Comments ($\triangleright$) reflect which restored constraint is made feasible.

Require: $\vec{X}^{*} \leftarrow \vec{X}$
  for $j \in \mathcal{J}^{\mathrm{S}}, t \in \mathcal{T}$ **do**
    $X^{\mathrm{ef}*}_{jt} \leftarrow \left(\frac{\bar{\eta}^{\mathrm{e}}_j - \mu_j \underline{\eta}^{\mathrm{e}}_j}{1-\mu_j}\right) - \left(\frac{\bar{\eta}^{\mathrm{e}}_j - \underline{\eta}^{\mathrm{e}}_j}{\hat{k}_j(1-\mu_j)}\right)\left(\frac{X^{\mathrm{p}*}_{jt}}{Y^{\mathrm{op}*}_{jt}}\right)$ if $Y^{\mathrm{op}*}_{jt} > 0$ $\underline{\eta}$ otherwise
$\triangleright$ Constraint (5)
    $X^{\mathrm{f}*}_{jt} \leftarrow \frac{X^{\mathrm{p}*}_{jt}}{X^{\mathrm{ef}*}_{jt}}$ if $Y^{\mathrm{op}*}_{jt} > 0$ 0 otherwise $\triangleright$ Constraint (6a)
  end for
  for $j \in (\mathcal{J}^{\mathrm{S}} \cap \mathcal{J}^{\mathrm{CHP}}), t \in \mathcal{T}$ **do**
    $\check{X}^{\mathrm{fl}*}_{jt} \leftarrow \gamma_j X^{\mathrm{f}*}_{jt}$ $\triangleright$ Constraint (9)
  end for
  if $\sum_{j \in \mathcal{J}^{\mathrm{CHP}}} Y^{\mathrm{a}}_j > 0$ **then**
    $X^{\mathrm{t}*}_1 \leftarrow \frac{\bar{\tau}+\hat{\tau}_j}{2}$ $\triangleright$ Set the initial temperature to the mid-point
    $X^{\mathrm{w}*} \leftarrow \underline{\nu}$ $\triangleright$ Constraint (10e)
    $\vec{X}^{*} \leftarrow$ THERMAL$(\vec{X}^{*})$
    while $\max\{X^{\mathrm{t}}_t\} > \bar{\tau}$ **do** $\triangleright$ Constraint (10b)
      $X^{\mathrm{w}*} \leftarrow X^{\mathrm{w}*} + \tilde{\nu}$
      $\bar{\nu} \leftarrow \bar{\nu} + \tilde{\nu}$ if $X^{\mathrm{w}*} > \bar{\nu}$ $\triangleright$ Constraint (10e)
      $\vec{X}^{*} \leftarrow$ THERMAL$(\vec{X}^{*})$
    end while
  else
    $\vec{X}^{*} \leftarrow$ NO CHP$(\vec{X}^{*})$
  end if

Function 1 - Creates feasibility for thermal energy constraints with combined-heat-and-power

  function THERMAL$(\vec{X}^{*})$
    for $t \in \mathcal{T}$ **do**
      $\check{Z}^{\mathrm{t}*}_t \leftarrow 1$ if $X^{\mathrm{t}*}_t \geq \check{\tau} + \epsilon$ 0 otherwise $\triangleright$ Constraint (10c)
      $\hat{Z}^{\mathrm{t}*}_t \leftarrow 1$ if $X^{\mathrm{t}*}_t \geq \hat{\tau}$ 0 otherwise $\triangleright$ Constraint (10d)
      $\hat{X}^{\mathrm{fl}*}_t \leftarrow \left(1 - \left[1 - \frac{\hat{\tau}_j - \underline{\tau}}{X^{\mathrm{t}*}_t - \underline{\tau}}\right]\hat{Z}^{\mathrm{t}*}_t\right)\frac{d^{\mathrm{h}}_t}{h^{\mathrm{w}}(\hat{\tau}_j - \check{\tau})}$ $\triangleright$ Constraint (2c)
      $X^{\mathrm{f}*}_{jt} \leftarrow \frac{h^{\mathrm{w}}\hat{X}^{\mathrm{fl}*}_t(\hat{\tau}_j - X^{\mathrm{t}*}_t)(1-\hat{Z}^{\mathrm{t}*}_t)}{\eta^{\mathrm{h}}_j}$ $j = \text{Boiler}$ $\triangleright$ Constraint (6c)
      $X^{\mathrm{t}*}_{t+1} \leftarrow (1 - \alpha\check{Z}^{\mathrm{t}*}_t)X^{\mathrm{t}*}_t + \frac{\Delta\sum_{j \in \mathcal{J}^{\mathrm{CHP}}} \eta^{\mathrm{h}}_j h^{\mathrm{e}}\check{X}^{\mathrm{fl}*}_{jt}(\hat{\tau}_j - X^{\mathrm{t}*}_t) - \Delta h^{\mathrm{w}}\hat{X}^{\mathrm{fl}*}_t(X^{\mathrm{t}*}_t - \check{\tau})}{(h^{\mathrm{w}}X^{\mathrm{w}*})}$
$\triangleright$ Constraint (10a)
    end for
    return $\vec{X}^{*}$
  end function

Journal: **11081** Article No.: **9844** TYPESET DISK LE CP Disp.:**2023/10/21** Pages: **35** Layout: **Small-Ex**

Function 2 - Creates feasibility for thermal energy constraints without combined-heat-and-power

function No CHP($\vec{X}^*$)
  $X_t^{t*} \leftarrow \check{\tau} \quad \forall t \in \mathcal{T}$ ▷ Constraints (10a), (10b)
  for $t \in \mathcal{T}$ **do**
    $\breve{Z}_t^{t*} \leftarrow 0$ ▷ Constraint (10c)
    $\hat{Z}_t^{t*} \leftarrow 0$ ▷ Constraint (10d)
    $\hat{X}_t^{fl*} \leftarrow \frac{d_t^h}{h^w(\hat{\tau}_j - \check{\tau})}$ ▷ Constraint (2c)
    $X_{jt}^{f*} \leftarrow \frac{h^w(\hat{\tau}_j - \check{\tau})\hat{X}_t^{fl*}}{\eta_j^h} \quad j = \text{Boiler}$ ▷ Constraint (6c)
  end for
  return $\vec{X}^*$
end function

4.3 Return of the original formulation ($\mathcal{P}'$) (Phase 3)

We reconstitute ($\mathcal{P}'$) by performing replacements of constraints in Table 3 consistent with transforming ($\mathcal{P}^\ell$) into ($\mathcal{P}'$). We use the solution obtained in **Phase 2** as a feasible starting point for ($\mathcal{P}'$). The solution to this problem provides an improvement over our initial feasible solution and, as a second-order effect, tightens the lower bound. To ensure that the resulting solution is feasible for ($\mathcal{P}'$), we assume that we have access to sufficient fuel for the boiler and to solid oxide fuel cells; we also assume that we can procure an appropriately sized hot water tank, which is necessary to maintain the water temperature within the allowable limits. The variables we update through Algorithm 1 are only found in the constraints we reinstate during **Phase 3**; through proper ordering of variable determination, we ensure feasibility. The remaining constraints, which are feasible for ($\mathcal{P}^\ell$), remain feasible with respect to ($\mathcal{P}'$).

5 Inputs and results

We solve ($\mathcal{P}'$) utilizing the process described in Sect. 4. This section describes the input data, provides the performance of the model in terms of solution quality and run time, and analyzes one such solution. Model ($\mathcal{P}'$) consists of a variety of inputs, including technology-specific data, electrical production factors, and electrical and heating loads.

5.1 General inputs

Table 4 provides parameter values for technologies other than fuel cells (Anderson et al. 2023b). (Sect. 5.2 describes inputs related to solid oxide fuel cells.)

We obtain all 16 distinct hourly electric load profiles for a representative year compiled by the National Renewable Energy Lab from the Open Energy Data Initiative website (https://openei.org/datasets/files/968/pub/individual_files/). This dataset was developed by the National Renewable Energy Lab's Distributed Energy Systems Inte-

Journal: 11081 Article No.: 9844 TYPESET DISK LE CP Disp.:2023/10/21 Pages: 35 Layout: Small-Ex

Table 4 Technology input values (not including solid oxide fuel cells)

Technology	Capital cost	O&M	Lifetime (years)
Photovoltaic	$1,592/kW	$17/ (kW year)	20
Lithium Ion Battery	$775/kWh	–	10
Generator	$500/kW	10/(kW year)	20
CHP System	$500/kW	0.019/kWh	20

CHP combined heat and power
The lithium-ion battery has a two-hour power rating

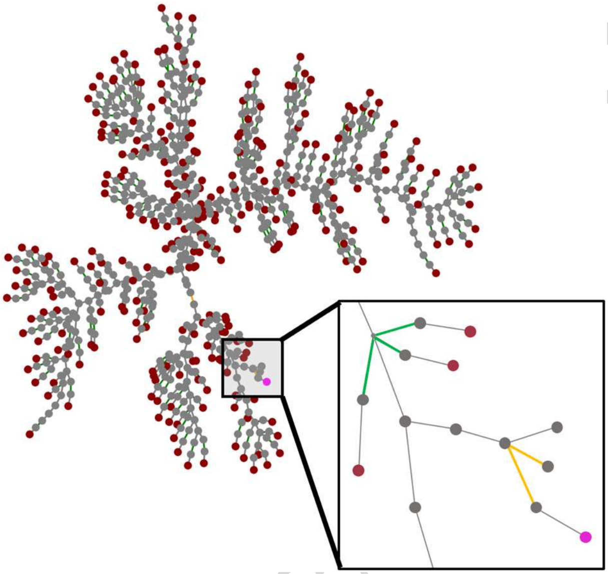

Fig. 7 R1-12.47-2 Taxonomy Feeder. Magenta represents the slack bus (the power source of the distribution network), while dark red depicts the loads that require power. Green links are transformers; orange links are switches; and gray links and nodes are triplex lines and connections, respectively

gration group as part of a study on high penetrations of distributed solar photovoltaics (Schneider et al. 2008). Table 10 in Appendix B provides details. We choose to highlight a moderate suburban community combined with a light rural area (R1-1247-2) to show how a microgrid consisting of solid oxide fuel cells can add resilience to communities at risk of fire-related utility service disruptions. Figure 7 is a snapshot of case R1-1247-2 (Cohen 2013).

Figure 8 depicts the load profile R1-1247-2. The oval in the figure shows the time period in which the natural disaster occurs and the corresponding unavailability of utility services. The dark blue color (outlined by the oval) shows that, for this particular instance, we reduce the demand to a predetermined "critical load" during the service disruption. We generate heating loads from the EnergyPlus® simulation software hosted by the National Renewable Energy Lab using a combination of five building types: hospital, hotel, apartment, large office, and supermarket. Figure 9 depicts a heat map of the thermal load at hourly fidelity. For the photovoltaic production factors f^{p}_{jt}, we use data obtained from the *PVWatts Tool* (Dobos 2014) given in Fig. 10. We anno-

Journal: 11081 Article No.: 9844 TYPESET DISK LE CP Disp.:2023/10/21 Pages: 35 Layout: Small-Ex

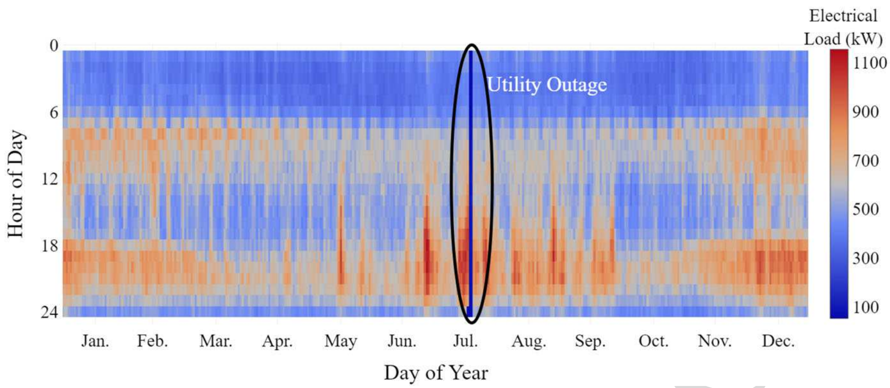

Fig. 8 Electric load profile for distribution feeder R1-1247-2, given by the network graph in Fig. 7, shown with a utility service disruption

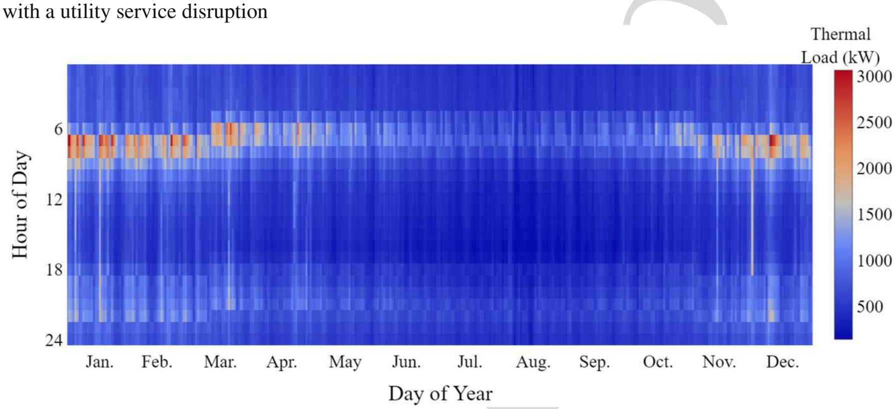

Fig. 9 Hot thermal load profile derived from the EnergyPlus® simulation software, representing a collection of building types, including a hospital, hotel, apartment, large office, and supermarket

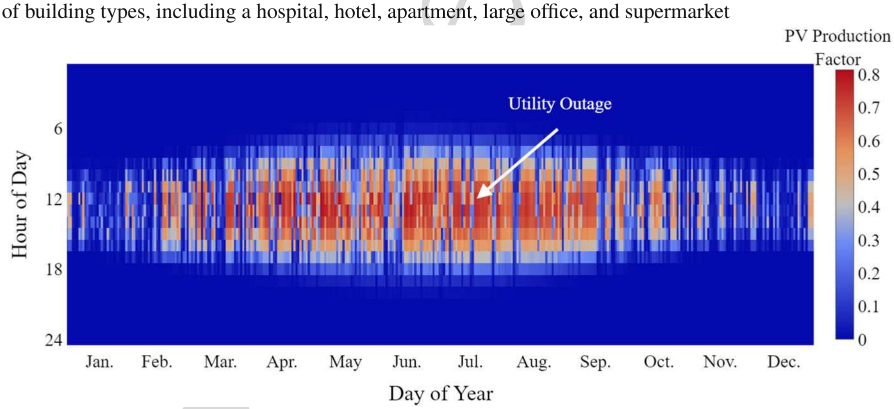

Fig. 10 Estimated electricity production of a grid-connected roof- or ground-mounted photovoltaic system installed in Richmond, CA. The arrow shows the approximate timeframe of the modeled utility service disruption

Journal: 11081 Article No.: 9844 TYPESET DISK LE CP Disp.:2023/10/21 Pages: 35 Layout: Small-Ex

tate the time of year during which the utility outage occurs to highlight the amount of solar irradiance available. The installed photovoltaic capacity for a resilience model is influenced by the outage time period selected.

5.2 Solid oxide fuel cell inputs

The U.S. Energy Information Administration (2020); Battelle Memorial Institute (2017a, b), and Whiston et al. (2021) offer costs associated with equipment, installation, stack, heat recovery, and inverters. We conduct analysis using system sizes from 10 to 250 kW. Cost values in this range are similar though minor differences exist between the 10–25 kW range (Battelle Memorial Institute 2017a) and the 100–250 kW range (Battelle Memorial Institute 2017b). A drawback of high-temperature solid oxide fuel cells is the cost associated with the stacks whose replacement is necessary, in part, due to the stress of operating at high temperatures (Whiston et al. 2021). Specifically, over time, the high-temperature gradients degrade the system. We therefore consider a conservative start-up (from ambient temperature) time of three hours (Ellamla et al. 2015) which assumes a heating rate of approximately 5°C per minute (Milcarek et al. 2018); in this way, we emphasize system reliability over fast start up. We incorporate fixed operations and maintenance (O&M) costs, including the cost of replacing the stack, reformer, and inverter after five years. System lifetime is assumed to be 10–20 years, depending on the source. Stack lifetime is assumed to be five years (Battelle Memorial Institute 2017a; 2017b, U.S. Energy Information Administration 2020, and Whiston et al. 2021).

Costs are separated into three categories (high, medium, and low). The high-capital-cost case assumes elevated equipment price and sales markup. Additionally, we consider variations by decade which are attributable to the assumption that an inverse relationship exists between production and price. We include a cost with sales markup for combined-heat-and-power heat recovery equipment and assume a 5% discount rate. See Appendix C for a more detailed description of the economic data.

We also update the efficiency parameters ($\bar{\eta}_j$ and $\underline{\eta}_j$) and start-up time (σ_j). To determine parameter values of interest, we vary them and solve the model to establish that, other than costs, the efficiency parameters and start-up time impact fuel cell

Table 5 Values used for power-only and combined-heat-and-power solid oxide fuel cells

Parameter	Description	Value	
		j =CHP	j =Power
$\bar{\eta}^{e}_j$	Maximum electricity efficiency	54%	54%
$\underline{\eta}^{e}_j$	Minimum electricity efficiency	60%	60%
σ_j	Start-up time for each technology j to reach μ_j	3 h	3 h
μ_j	Maximum turn-down	20%	20%
$\bar{\kappa}_j$	Capital cost	\$3,360/kW	\$2,800/kW
c^{om}_j	O&M cost	\$0.024/kWh	\$0.020/kWh

Journal: 11081 Article No.: 9844 TYPESET DISK LE CP Disp.:2023/10/21 Pages: 35 Layout: Small-Ex

operational behavior the most. Beigzadeh et al. (2021) report electrical efficiencies of solid oxide fuel cells between 57 and 72%, depending on the type of fuel used; the lower value corresponds to gasified biomass and the higher to natural gas. Additionally, we confirm, through discussion with commercial partners, that deployed systems realize electrical efficiencies of around 60%. We use conservative values to account for both lifecycle system degradation and the utilization of biofuel. However, an end-user of our framework could choose to modify these values as the technology continues to mature. Table 5 reflects parameter values that differ from Pruitt et al. (2014).

5.3 Model inputs from solution-expediting methodologies

Figure 11 shows how the bound tightening procedure (Pruitt et al. 2014) produces desired reductions in variable bounds for those variables appearing in bi-linear terms. These reductions allow the spatial branch-and-bound algorithm to find better solutions and tighten the bound on the optimal objective function value more easily.

We compare the size of models $(\mathcal{P}')$ and $(\mathcal{P}^{\ell})$, for the inputs used, in Table 6. Model $(\mathcal{P}')$ contains over 275,000 constraints, of which 52,000 involve non-linear terms. The reduced size and complexity of $(\mathcal{P}^{\ell})$ relative to $(\mathcal{P}')$ affords us with the ability to generate good solutions quickly, with which we can then initialize the original monolith.

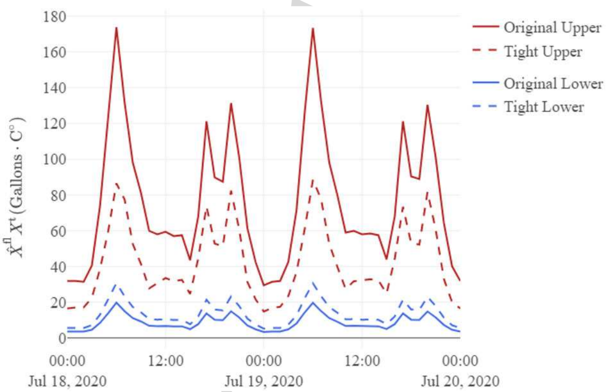

Fig. 11 Improvement from bound-tightening procedure for the auxiliary, bi-linear term $\hat{X}^{\text{fl}}_{jt} \cdot X^{\text{t}}_{t}$ reduces the magnitude between the upper and lower bound by 57%, as an example

Table 6 Average size and structure of models $(\mathcal{P}')$ and $(\mathcal{P}^{\ell})$. The $(\mathcal{P}^{\ell})$ column shows the percent increase or decrease in size relative to $(\mathcal{P}')$

Category	Type	$(\mathcal{P}')$	$(\mathcal{P}^{\ell})$ %
Variables	Total	232,034	-15
	Continuous	179,478	-20
	Discrete	52,556	0
Constraints	Total	275, 897	0
	Linear	223,339	24
	Non-linear	52,558	-100

Journal: 11081 Article No.: 9844 TYPESET DISK LE CP Disp.:2023/10/21 Pages: 35 Layout: Small-Ex

5.4 Solution quality

Solving ($\mathcal{P}'$) using ($\mathbf{M}^e$) yields solutions, on average, five times faster than solving ($\mathcal{P}'$) using ($\mathbf{M}^b$). Table 7 shows results for a one-year time horizon. In general, ($\mathbf{M}^e$) generates an 8% improvement in the objective function value and over a 50% improvement in the optimality gap after a two-hour solve time limit. In only one of the 16 instances did ($\mathbf{M}^b$) return the first solution faster; however, even in this case, the solution obtained by ($\mathbf{M}^e$) is superior.

Table 7 Comparison of solutions solving ($\mathcal{P}'$) with and without the solution obtained from ($\mathcal{P}^{\ell}$)

Case	Objective function value decrease ($)			Optimality gap reduction (%)			Time to first solution (Seconds)		
	($\mathbf{M}^b$)	($\mathbf{M}^e$)	% Δ	($\mathbf{M}^b$)	($\mathbf{M}^e$)	% Δ	($\mathbf{M}^b$)	($\mathbf{M}^e$)	Δ
R1-1247-2	1,012,986	931,014	8	15	7	50	178	56	122
R1-1247-3	745,548	692,023	7	14	7	48	253	56	197
R1-1247-4	2,164,754	1,906,774	12	18	7	62	377	73	304
R1-2500-1	1,556,543	1,412,495	9	16	7	54	503	63	440
R2-1247-1	4,483,279	4,112,745	8	13	5	61	845	63	782
R2-1247-2	3,269,277	2,971,911	9	15	6	58	298	60	238
R2-2500-1	7,825,518	7,379,453	6	10	4	57	748	68	680
R3-1247-2	4,085,636	3,790,034	7	13	6	54	1042	63	979
R4-1247-2	1,744,135	1,589,823	9	15	7	53	288	47	241
R4-2500-1	1,914,215	1,742,076	9	15	7	55	295	75	220
R5-1247-1	6,076,208	5,414,754	11	15	5	68	471	69	402
R5-1247-2	4,500,123	4,165,739	7	13	6	56	911	73	838
R5-1247-4	4,470,154	4,017,051	10	15	5	64	232	69	163
R5-1247-5	4,165,565	3,835,660	8	13	5	58	313	181	132
R5-2500-1	7,932,270	7,272,899	8	12	4	66	240	356	(116)
R5-3500-1	5,425,448	5,078,233	6	11	5	56	425	75	350
Average across all cases			8	14	6	58	464	90	373

Objective function values and optimality gap after two hours of run time, and time until the first feasible solution is obtained. Δ: Reduction between methods ($\mathbf{M}^b$) and ($\mathbf{M}^e$)

5.5 Solution implications

To assess the financial benefits of distributed generation, we compare the solution with no distributed generation to that with an installed microgrid capable of servicing a critical load during a utility service disruption. In order to create an equitable comparison, we omit the energy cost during the service disruption. Table 8 depicts the resulting values for all 16 load profiles, along with the fraction of demanded power serviced from the utility in the presence of a microgrid. In all cases, the cost to meet the demanded electrical load with distributed generation is less than that associated with the “No Microgrid” solution. Along with cost savings of 8.3%, on average, across

Journal: 11081 Article No.: 9844 TYPESET DISK LE CP Disp.:2023/10/21 Pages: 35 Layout: Small-Ex

Table 8 Solution comparison between purchasing all electricity from the utility versus installing a microgrid that is capable of meeting a 48-hour outage occurring during the highest electrical demand period

Case	Annualized lifecycle cost ($)		Δ	Grid
	No microgrid	Microgrid	(%)	Utilization (%)
R1-1247-2	1,007,933	929,337	−8.5	12.4
R1-1247-3	731,736	690,028	−6.0	6.5
R1-1247-4	2,115,108	1,903,575	−11.1	13.1
R1-2500-1	1,545,364	1,408,578	−9.7	8.1
R2-1247-1	4,419,348	4,101,889	−7.7	10.8
R2-1247-2	3,239,292	2,969,497	−9.1	15.2
R2-2500-1	7,916,373	7,366,441	−7.5	15.2
R3-1247-2	4,058,615	3,775,831	−7.5	8.9
R4-1247-2	1,731,984	1,587,963	−9.1	24.0
R4-2500-1	1,910,583	1,740,579	−9.8	20.3
R5-1247-1	5,832,474	5,402,292	−8.0	13.8
R5-1247-2	4,503,345	4,154,198	−8.4	7.4
R5-1247-4	4,343,550	4,009,787	−8.3	16.6
R5-1247-5	4,136,660	3,831,042	−8.0	21.5
R5-2500-1	7,763,028	7,263,047	−6.9	19.7
R5-3500-1	5,448,520	5,071,643	−7.4	20.3

Table 9 Percent of total power consumed during the year by each type of installed technology in the microgrid

Case	Dispatched power (%)			
	CHP SOFC	Power SOFC	PV	Utility
R1-1247-2	88	0	0	12
R1-1247-3	89	0	5	6
R1-1247-4	86	0	1	13
R1-2500-1	84	0	8	8
R2-1247-1	47	35	8	10
R2-1247-2	65	20	0	15
R2-2500-1	25	57	3	15
R3-1247-2	51	36	4	9
R4-1247-2	76	0	0	24
R4-2500-1	80	0	0	20
R5-1247-1	35	51	1	13
R5-1247-2	45	45	3	7
R5-1247-4	48	36	0	16
R5-1247-5	51	28	0	21
R5-2500-1	26	55	0	19
R5-3500-1	38	42	0	20
Average	59	25	2	14

No solution includes the diesel generator. *CHP* combined heat and power, *SOFC* solid oxide fuel cell, *PV* photovoltaics

Journal: 11081 Article No.: 9844 TYPESET DISK LE CP Disp.:2023/10/21 Pages: 35 Layout: Small-Ex

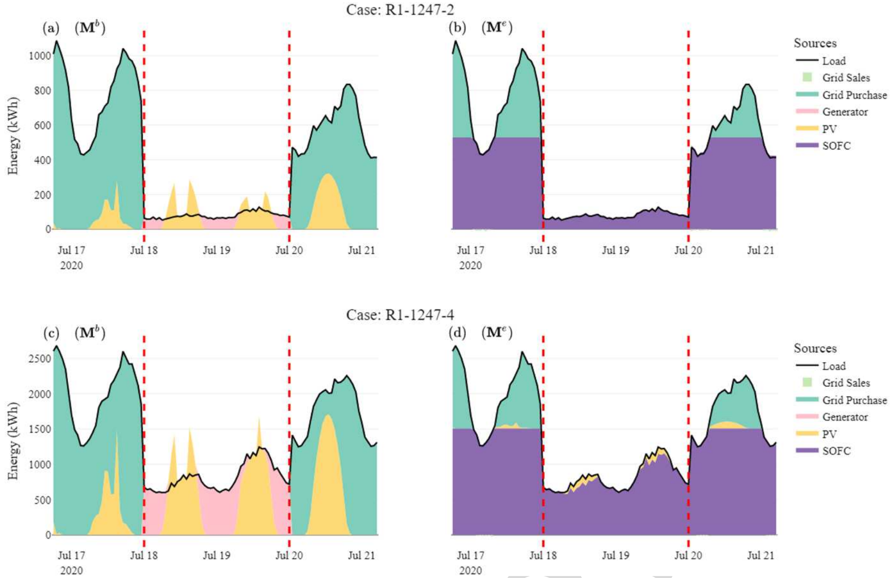

Fig. 12 Power output by technology type from a combination of microgrid and utility. Dashed lines show the start and end of the utility service disruption. Omitted from the plots are electrical storage operations; while they are part of the configuration, they are not utilized during the depicted time frame. Grid sales are present directly proceeding the outage but are difficult to discern

the 16 cases, the customer also benefits from added reliability and resilience by being able to service the electrical load during power disruptions to the utility.

Table 9 reflects the dispatched amount of each technology as a percentage of the total power consumed throughout the year. All remaining power is met by the utility. For almost all 16 cases, the co-generational fuel cell dominates the other technologies in dispatched power, providing approximately 58% of demanded annual power, with an additional 25% coming from the power-only fuel cell. Additionally, because this is a hybrid system of solid oxide fuel cells, photovoltaics, and electrical storage, the diesel generator is not consistently relied on to provide power. This mix of installed technologies also enhances system reliability in that there is not a single point of failure. An additional benefit of the installed microgrid is sustaining possible disruptions in fuel supply. Solid oxide fuel cells have the ability to utilize bio-fuels and, therefore, if strategically located at a site that produces bio-waste, the fuel cell would have access to low-cost fuel that is sourced on-site. This type of setup would reduce the dependency on utility-provided fuel sources while increasing the overall resilience and reliability of the system.

Figure 12 compares, for two representative instances (R1-1247-2 and R1-1247-4—highlighted in gray in Table 8), solutions returned by ($\mathbf{M}^b$) and ($\mathbf{M}^e$). These two instances differ by electric demand, in which the former services a smaller critical load during the outage than the latter. The area between the two dashed red lines represents the grid outage. We require the model to service the fully demanded electric and heating load during the disruption. Plots (a) and (c) show the solution returned by ($\mathbf{M}^b$), in which the solver is unable to leverage the benefit of a combined-heat-and-power solid

Journal: 11081 Article No.: 9844 TYPESET DISK LE CP Disp.:2023/10/21 Pages: 35 Layout: Small-Ex

oxide fuel cell, resulting in larger objective function values (shown in Table 7). Instead, the solution installs an oversized photovoltaic system and a backup diesel generator. While this is an acceptable alternative to adding resilience to the system, the solution favors traditional methods. Plots (b) and (d) reflect solutions obtained by ($\mathbf{M}^e$) which correspond to comparatively smaller objective function values while leveraging co-generational technologies. Additionally, the solutions returned by ($\mathbf{M}^e$) do not result in curtailed power during the outage.

6 Conclusion

This work demonstrates an optimization-based framework for creating solutions that enhance community resilience during outages by increasing the reliability of the electrical infrastructure. We present a mixed-integer, non-linear optimization model that incorporates many distributed energy resource technologies. Our model ($\mathcal{P}'$) is a member of a class of problems (mixed-integer nonlinear programs) that often present challenges for commercial optimization solvers. Therefore, we create a methodology capable of quickly generating solutions with better objective function values.

The framework presented affords civic and governmental organizations the ability to develop alternate solutions to meet their electric power needs during a utility service disruption and to provide critical services in post-disaster recovery. Additionally, we show the benefit of incorporating solid oxide fuel cells into a microgrid design, due, in part, to its minimal emissions, dependable power supply, and ability to consume multiple fuel types.

Acknowledgements This work is a collaborative effort between the Colorado School of Mines, Carnegie Mellon University, Bentley University, and industry partners, in particular, Martin Hering from Robert Bosch LLC. We acknowledge contributions from Dr. Amritanshu Pandey of the University of Vermont and Arnav Gautam from Carnegie Mellon University for their assistance in modeling and representing the distribution network. We thank Leonardo Aragon and Ty Gonzalez of the Colorado School of Mines for their data collection efforts. And, we are grateful for the technical expertise of Dr. Jack Brouwer of the University of California-Irvine regarding the fuel cells. The project is funded by the National Science Foundation grant number 2053856.

Appendix A: Disaster cost components

More than one dozen public and private sector data sources help capture the total, direct costs (both insured and uninsured) of the weather and climate events. These costs include physical damage to residential, commercial, and municipal buildings; material assets (content) within buildings; time element losses such as business interruption or loss of living quarters; damage to vehicles and boats; public assets including roads, bridges, levees; electrical infrastructure and offshore energy platforms; agricultural assets including crops, livestock, and commercial timber; and wildfire suppression costs, among others. However, these disaster costs do not take into account losses to natural capital or environmental degradation; mental or physical healthcare-related costs, the value of a statistical life; or supply chain, contingent business interruption costs. Therefore, our estimates should be considered conservative with respect to what

Journal: 11081 Article No.: 9844 TYPESET DISK LE CP Disp.:2023/10/21 Pages: 35 Layout: Small-Ex

is truly lost, but cannot be completely measured due to a lack of consistently available data (Smith 2021).

Appendix B: Taxonomy feeders

See Table 10.

Table 10 Summary of distribution feeders used to create electrical load profile

Feeder	Community description	Annual electrical demand (kWh)
R1-1247-2	Moderate suburban and light rural	4,905,544
R1-1247-3	Small urban center	2,589,839
R1-1247-4	Heavy suburban	14,586,540
R1-2500-1	Light rural	9,577,933
R2-1247-1	Light urban	34,316,316
R2-1247-2	Moderate suburban	24,148,877
R2-2500-1	Moderate urban	64,973,641
R3-1247-2	Moderate urban	31,760,229
R4-1247-2	Light suburban and moderate urban	11,047,930
R4-2500-1	Light rural	12,409,270
R5-1247-1	Heavy suburban and moderate urban	47,010,268
R5-1247-2	Moderate suburban and heavy urban	35,584,108
R5-1247-4	Moderate suburban and urban	33,908,450
R5-1247-5	Moderate suburban and light urban	31,886,294
R5-2500-1	Heavy suburban and moderate urban	63,259,096
R5-3500-1	Moderate suburban and light urban	43,247,521

Data obtained from the Open Energy Data Initiative https://openei.org/datasets/files/968/pub/individual_files/ and sourced from work by Schneider et al. (2008)

Appendix C: Additional solid oxide fuel cell costs

Assumptions

- U.S. Energy Information Administration (2020) estimates "owner costs" though the applicability of those to this context is unclear: "typically include development costs, preliminary feasibility and engineering studies, environmental studies and permitting, legal fees, project management (including third-party management), insurance costs, infrastructure interconnection costs (e.g., gas, electricity), and owner's contingency."
- O&M costs from U.S. Energy Information Administration (2020) are orders of magnitude different from Battelle Memorial Institute (2017a) as the former estimates are much more inclusive.
- High capital cost case assumes high equipment costs and a high sales markup.

Journal: 11081 Article No.: 9844 TYPESET DISK LE CP Disp.:2023/10/21 Pages: 35 Layout: Small-Ex

Table 11 Projected costs of solid oxide fuel cells

Scenario Production (units/yr)		2020 100–500	2030 500–1 k	2040 1–10 k	2050 10–50 k
Capital cost ($/kW)	High	17,245	7221	5068	4967
	Medium	5425	4318	3007	2712
	Low	2384	1946	1902	1813
Equipment cost ($/kW)	High	16,000	6000	3896	3,818
	Medium	4800	3818	2557	2312
	Low	1984	1546	1502	1413
CHP equipment cost ($/kW)	High*	934	795	731	692
	Medium	471	462	453	444
	Low	167	162	157	148
Installation cost ($/kW)	High	1245	1221	1172	1149
	Medium	625	500	450	400
	Low*	400	400	400	400
FOM ($/kW/yr)	High	318	318	318	318
	Medium	217	156	147	133
	Low	167	138	129	116
VOM ($/kWh)	High	0.092	0.090	0.088	0.086
	Medium	0.047	0.046	0.045	0.044
	Low	0.002	0.002	0.002	0.002
$LCOE_{ij}$ ($/kWh)	High	0.405	0.244	0.207	0.204
	Medium	0.160	0.134	0.111	0.103
	Low	0.060	0.050	0.048	0.045

*Represents cost values for systems of projected size of 50 kW or less. *CHP* combined heat and power, *FOM* Fixed operations and maintenance cost, *VOM* variable operations and maintenance cost

- Costs over time are based on the assumption that production volumes increase, reducing the costs of production.
- Equipment cost includes the cost of heat recovery equipment for combined heat and power and sales markup.
- Costs assume a 5% discount rate, but given current economic conditions, a higher value may be more appropriate and would increase the low and medium case fixed O&M.
- With all sources pooled together, there was agreement that production volume matters for costs, but not system size (except at very small system sizes, 1 kW and 5 kW, which we do not consider in the model).
- The levelized cost of energy (LCOE) estimates only factor in the electricity delivered, not the heat energy, assuming a 5% discount rate, a 10-year system lifetime, a 5-year stack and inverter replacement, and a capacity factor of 93%.

Based on these assumptions, we estimate fuel cell costs and report them in Table 11.

Journal: 11081 Article No.: 9844 TYPESET DISK LE CP Disp.:2023/10/21 Pages: 35 Layout: Small-Ex

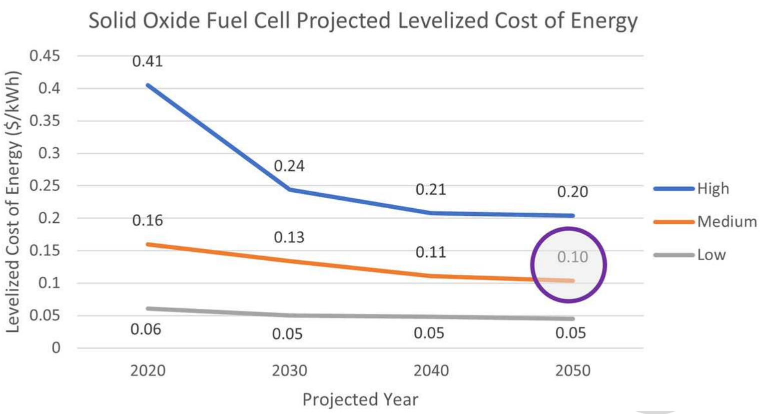

Fig. 13 Projected levelized cost of energy for power-only solid oxide fuel cells. Projections extend to 2050 based on the values found in Table 11

LCOE_{Nj} is the levelized cost of energy for technology j, at a life expectancy of N, where AEP is the annual electricity production, and is computed as:

$$\mathrm{LCOE}_{ij} = \frac{\kappa_j \frac{i(1+i)^{N_j}}{(1+i)^{N_j}-1} + \mathrm{FOM}}{\mathrm{AEP}} + \mathrm{VOM}$$

Figure 13 shows the projected costs over time for each category: high, medium, and low. The purple circle shows the value we use for our modeling efforts.

References

Abiodun K, Gautam A, Newman A, Nock D, Pandey A (2022) The role of microgrids in advancing energy equity through access and resilience. In: Tutorials in operations research: emerging and impactful topics in operations, pp 175–190

Anderson KH, Cutler DS, Olis DR, Elgqvist EM, Li X, Laws ND, DiOrio NA, Walker HA (2017) REopt: a platform for energy system integration and optimization. Technical Report NREL/TP-7A40-70022, National Renewable Energy Lab. (NREL), Golden. https://doi.org/10.2172/1395453. https://www.osti.gov/biblio/1395453

Anderson K, Grymes J, Warren A, Newman A (2023a) North Carolina water utility builds resilience with distributed energy resources. INFORMS J Appl Anal 53:247–265

Anderson K, Olis D, Becker B, Parkhill L, Laws N, Li X, Mishra S, Jeffery A, Elgqvist E, Krah K, Cutler D, Zolan A, Muerdter N, Eger R, Walker A, Hampel C, Tomberlin G, Farthing A (2023b) The REopt Web Tool User Manual. Technical report, National Renewable Energy Laboratory

Arefifar SA, Yasser ARM, El-Fouly TH (2013) Optimum microgrid design for enhancing reliability and supply-security. IEEE Trans Smart Grid 4(3):1567–1575. https://doi.org/10.1109/TSG.2013.2259854

Aziz AS, Tajuddin MFN, Hussain MK, Adzman MR, Ghazali NH, Ramli MAM, Zidane TEK (2022) A new optimization strategy for wind/diesel/battery hybrid energy system. Energy 239:122458. https://doi.org/10.1016/j.energy.2021.122458

Balas E (1965) An additive algorithm for solving linear programs with zero-one variables. Oper Res 13(4):517–546. https://doi.org/10.1287/opre.13.4.517

Baldinelli A, Barelli L, Bidini G, Cinti G (2021) Micro-cogeneration based on solid oxide fuel cells: Market opportunities in the agriculture/livestock sector. Int J Hydrog Energy 46(16):10036–10048. https://doi.org/10.1016/j.ijhydene.2020.04.226

Journal: 11081 Article No.: 9844 TYPESET DISK LE CP Disp.:2023/10/21 Pages: 35 Layout: Small-Ex

Battelle Memorial Institute (2017a) Manufacturing cost analysis of 1, 5, 10 and 25 kW fuel cell systems for primary power and combined heat and power applications. Technical report, Battelle Memorial Institute

Battelle Memorial Institute (2017b) Manufacturing cost analysis of 100 and 250 kW fuel cell systems for primary power and combined heat and power applications. Technical report, Battelle Memorial Institute

Beigzadeh M, Pourfayaz F, Ghazvini M, Ahmadi MH (2021) Energy and exergy analyses of solid oxide fuel cell-gas turbine hybrid systems fed by different renewable biofuels: a comparative study. J Clean Prod 280:124383. https://doi.org/10.1016/j.jclepro.2020.124383

Bernal-Agustín JL, Dufo-López R, Rivas-Ascaso DM (2006) Design of isolated hybrid systems minimizing costs and pollutant emissions. Renew Energy 31(14):2227–2244. https://doi.org/10.1016/j.renene.2005.11.002

Campbell RJ (2012) Weather-related power outages and electric system resiliency. Congr Res J

Center for Climate and Energy Solutions (2020) https://www.c2es.org/content/microgrids/

Chapin FS, Trainor SF, Huntington O, Lovecraft AL, Zavaleta E, Natcher DC, McGuire AD, Nelson JL, Ray L, Calef M, Fresco N, Huntington H, Rupp TS, DeWilde L, Naylor RL (2008) Increasing wildfire in Alaska's boreal forest: pathways to potential solutions of a wicked problem. BioScience 58(6):531–540. https://doi.org/10.1641/B580609

Climate Central (2020) https://www.climatecentral.org/climate-matters/power-outages

Cohen MA (2013). http://emac.berkeley.edu/gridlabd/taxonomy_graphs/

Davies IP, Haugo RD, Robertson JC, Levin PS (2018) The unequal vulnerability of communities of color to wildfire. PLoS ONE 13(11):0205825. https://doi.org/10.1371/journal.pone.0205825

Deng Q, Gao X, Zhou H, Hu W (2011) System modeling and optimization of microgrid using genetic algorithm. In: 2011 2nd international conference on intelligent control and information processing, vol 1, pp 540–544. https://doi.org/10.1109/ICICIP.2011.6008303

Department of Energy (2018) Department of Energy Report Explores U.S. Advanced Small Modular Reactors to Boost Grid Resiliency. https://www.energy.gov/ne/articles/department-energy-report-explores-us-advanced-small-modular-reactors-boost-grid

Dobos A (2014) PVWatts version 5 manual. Technical Report NREL/TP-6A20-62641, 1158421. National Renewable Energy Lab. https://doi.org/10.2172/1158421. http://www.osti.gov/servlets/purl/1158421/

Donaldson DL, Alvarez-Alvarado MS, Jayaweera D (2020) Power system resiliency during wildfires under increasing penetration of electric vehicles. In: 2020 International conference on probabilistic methods applied to power systems (PMAPS), pp 1–6. https://doi.org/10.1109/PMAPS47429.2020.9183683

Ellamla HR, Staffell I, Bujlo P, Pollet BG, Pasupathi S (2015) Current status of fuel cell based combined heat and power systems for residential sector. J Power Sources 293:312–328. https://doi.org/10.1016/j.jpowsour.2015.05.050

Goodall G, Scioletti M, Zolan A, Suthar B, Newman A, Kohl P (2019) Optimal design and dispatch of a hybrid microgrid system capturing battery fade. Optim Eng 20:179–213

Greene N, Hammerschlag R (2000) Small and clean is beautiful: exploring the emissions of distributed generation and pollution prevention policies. Electr J 13(5):50–60. https://doi.org/10.1016/S1040-6190(00)00118-4

Jenkins T (2018) Impacts of the 2017 wildfires in the United States. https://www.govinfo.gov/committee/house-transportation?path=/browsecommittee/chamber/house/committee/transportation

Jolly WM, Cochrane MA, Freeborn PH, Holden ZA, Brown TJ, Williamson GJ, Bowman DMJS (2015) Climate-induced variations in global wildfire danger from 1979 to 2013. Nat Commun 6(11):7537. https://doi.org/10.1038/ncomms8537

Kocatepe A, Ulak MB, Kakareko G, Ozguven EE, Jung S, Arghandeh R (2019) Measuring the accessibility of critical facilities in the presence of hurricane-related roadway closures and an approach for predicting future roadway disruptions. Nat Hazards 95:615–635

Lambert T (2000) HOMER® Energy modeling software, version 00. Technical report, National Renewable Energy Lab. (NREL), Golden. https://www.osti.gov/biblio/1231441

Lin Y, Bie Z, Qiu A (2018) A review of key strategies in realizing power system resilience. Glob Energy Interconnect 1(1):70–78

Milcarek RJ, Garrett MJ, Welles TS, Ahn J (2018) Performance investigation of a micro-tubular flame-assisted fuel cell stack with 3000 rapid thermal cycles. J Power Sources 394:86–93. https://doi.org/10.1016/j.jpowsour.2018.05.060

Mishra S, Anderson K, Miller B, Boyer K, Warren A (2020) Microgrid resilience: a holistic approach for assessing threats, identifying vulnerabilities, and designing corresponding mitigation strategies. Appl Energy 264:114726. https://doi.org/10.1016/j.apenergy.2020.114726

Molinari NA, Chen B, Krishna N, Morris T (2017) Who's at risk when the power goes out? The at-home electricity-dependent population in the United States

Morais H, Kádár P, Faria P, Vale ZA, Khodr HM (2010) Optimal scheduling of a renewable micro-grid in an isolated load area using mixed-integer linear programming. Renew Energy 35(1):151–156. https://doi.org/10.1016/j.renene.2009.02.031

Newburger E (2019) More than 2 million people expected to lose power in PG&E blackout as California wildfires rage. https://www.cnbc.com/2019/10/26/pge-will-shut-off-power-to-940000-customers-in-northern-california-to-reduce-wildfire-risk.html

Nilsson H (2023) https://www.utilitydive.com/news/us-microgrid-market-wood-mackenzie/642341/

Pacific Gas and Electric (2021) Backup power. https://www.pge.com/en_US/safety/electrical-safety/electric-generator-safety/electric-generator-safety.page

Palaiologou P, Ager AA, Nielsen-Pincus M, Evers CR, Day MA (2019) Social vulnerability to large wildfires in the western USA. Landsc Urban Plan 189:99–116. https://doi.org/10.1016/j.landurbplan.2019.04.006

Pruitt KA, Leyffer S, Newman AM, Braun RJ (2014) A mixed-integer nonlinear program for the optimal design and dispatch of distributed generation systems. Optim Eng 15(1):167–197. https://doi.org/10.1007/s11081-013-9226-6

Qazi SH, Mustafa MW, Sultana U, Mirjat NH, Soomro SA, Rasheed N (2018) Regulation of voltage and frequency in solid oxide fuel cell-based autonomous microgrids using the whales optimisation algorithm. Energies 11(55):1318. https://doi.org/10.3390/en11051318

Rehman S, Al-Hadhrami LM (2010) Study of a solar PV-diesel-battery hybrid power system for a remotely located population near Rafha, Saudi Arabia. Energy 35(12):4986–4995. https://doi.org/10.1016/j.energy.2010.08.025

Schneider KP, Chen Y, Chassin DP, Pratt RG, Engel DW, Thompson SE (2008) Modern grid initiative distribution taxonomy final report. Technical Report PNNL-18035, 1040684, Pacific Northwest National Lab. https://doi.org/10.2172/1040684. http://www.osti.gov/servlets/purl/1040684/

Schoennagel T, Balch JK, Brenkert-Smith H, Dennison PE, Harvey BJ, Krawchuk MA, Mietkiewicz N, Morgan P, Moritz MA, Rasker R, Turner MG, Whitlock C (2017) Adapt to more wildfire in western North American forests as climate changes. Proc Natl Acad Sci 114(18):4582–4590. https://doi.org/10.1073/pnas.1617464114

Scioletti MS, Newman AM, Goodman JK, Zolan AJ, Leyffer S (2017) Optimal design and dispatch of a system of diesel generators, photovoltaics and batteries for remote locations. Optim Eng 18:755–792

Shokoohi S, Golshannavaz S, Khezri R, Bevrani H (2018) Intelligent secondary control in smart microgrids: an on-line approach for islanded operations. Optim Eng 19:917–936

Smith AB (2021) 2021 U.S. billion-dollar weather and climate disasters. http://www.climate.gov/news-features/blogs/beyond-data/2021-us-billion-dollar-weather-and-climate-disasters-historical

Sorrentino M, Adamo A, Nappi G (2019) Optimal sizing of an rSOC-based renewable microgrid. Energy Procedia 159:237–242. https://doi.org/10.1016/j.egypro.2018.12.063

U.S. Department of Energy (2023) U.S. Department of Energy, Form OE-417. https://www.oe.netl.doe.gov/OE417_annual_summary.aspx

U.S. Energy Information Administration (2020) Distributed generation, battery storage, and combined heat and power system characteristics and costs in the buildings and industrial sectors. Technical report, U.S. Energy Information Administration

USAToday (2018) Natural disasters: California Camp Fire was world's costliest in 2018. https://www.usatoday.com/story/news/2019/01/08/natural-disasters-camp-fire-worlds-costliest-catastrophe-2018/2504865002/

Vigneysh T, Kumarappan N (2016) Autonomous operation and control of photovoltaic/solid oxide fuel cell/battery energy storage based microgrid using fuzzy logic controller. Int J Hydrog Energy 41(3):1877–1891. https://doi.org/10.1016/j.ijhydene.2015.11.022

Whiston MM, Lima Azevedo IM, Litster S, Samaras C, Whitefoot KS, Whitacre JF (2021) Paths to market for stationary solid oxide fuel cells: expert elicitation and a cost of electricity model. Appl Energy 304:117641. https://doi.org/10.1016/j.apenergy.2021.117641

Journal: 11081 Article No.: 9844 TYPESET DISK LE CP Disp.:2023/10/21 Pages: 35 Layout: Small-Ex

Zolan AJ, Scioletti MS, Morton DP, Newman AM (2021) Decomposing loosely coupled mixed-integer programs for optimal microgrid design. INFORMS J Comput 33(4):1300–1319. https://doi.org/10.1287/ijoc.2020.0955

Publisher's Note Springer Nature remains neutral with regard to jurisdictional claims in published maps and institutional affiliations.

Journal: **11081** Article No.: **9844** TYPESET DISK LE CP Disp.:**2023/10/21** Pages: **35** Layout: **Small-Ex**